

Journal Pre-proofs

Design, Synthesis and Molecular Modeling of Phenyl Dihydropyridazinone Derivatives as B-Raf Inhibitors with Anticancer Activity

Mohamed G. Thabit, Amany S. Mostafa, Khalid B. Selim, Magda A. A. Elsayed, Magda N. A. Nasr

PII: S0045-2068(20)31445-0
DOI: <https://doi.org/10.1016/j.bioorg.2020.104148>
Reference: YBIOO 104148

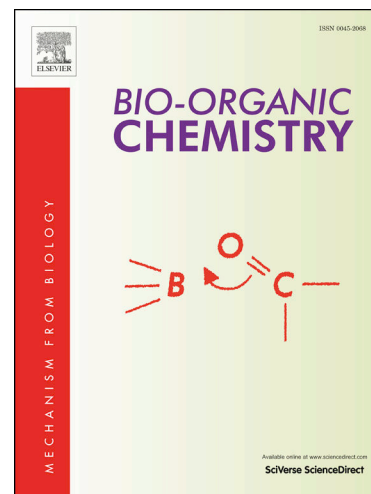
To appear in: *Bioorganic Chemistry*

Received Date: 26 November 2019
Revised Date: 25 June 2020
Accepted Date: 26 July 2020

Please cite this article as: M.G. Thabit, A.S. Mostafa, K.B. Selim, M. A. A. Elsayed, M. N. A. Nasr, Design, Synthesis and Molecular Modeling of Phenyl Dihydropyridazinone Derivatives as B-Raf Inhibitors with Anticancer Activity, *Bioorganic Chemistry* (2020), doi: <https://doi.org/10.1016/j.bioorg.2020.104148>

This is a PDF file of an article that has undergone enhancements after acceptance, such as the addition of a cover page and metadata, and formatting for readability, but it is not yet the definitive version of record. This version will undergo additional copyediting, typesetting and review before it is published in its final form, but we are providing this version to give early visibility of the article. Please note that, during the production process, errors may be discovered which could affect the content, and all legal disclaimers that apply to the journal pertain.

© 2020 Published by Elsevier Inc.



Design, Synthesis and Molecular Modeling of Phenyl Dihydropyridazinone Derivatives as B-Raf Inhibitors with Anticancer Activity

Mohamed G. Thabit,¹ Amany S. Mostafa,¹ Khalid B. Selim,^{1,*} Magda A. A. Elsayed^{1,2} and Magda N. A. Nasr¹

¹*Department of Pharmaceutical Organic Chemistry, Faculty of Pharmacy, Mansoura University, Mansoura 35516, Egypt*

²*Department of Pharmaceutical Chemistry, Faculty of Pharmacy, Horus University, New Dammeitta, Egypt*

*Corresponding author: K. B. Selim (e-mail: khbselim@mans.edu.eg)
tel: +2050-2247496 fax: +2050-2247496

Abstract

Three new series of phenyl dihydropyridazinone derivatives **4b–8i** have been designed, synthesized and evaluated for their anticancer activity against different cancer cell lines. Nine compounds showed strong inhibitory activity, among which compound **8b** exhibited potent activity against PC-3 cell line with IC₅₀ value of 7.83 μ M in comparison to sorafenib (IC₅₀ 11.53 μ M). Compounds **6a**, **6c**, **7f–h** and **8a–d** were further screened for their B-Raf inhibitory activity where seven compounds **7f–h** and **8a–d** showed high B-Raf inhibition with ranges of IC₅₀ values 70.65–84.14 nM and 24.97–44.60 nM, respectively when compared to sorafenib (IC₅₀ 44.05 nM). Among the tested compounds, **8b** was the most potent B-Raf inhibitor with IC₅₀ value of 24.79 nM. Cell cycle analysis of MCF-7 cells treated with **8b** showed cell cycle arrest at G2-M phase with significant apoptotic effect. Molecular modeling study was performed to understand the binding mode of the most active synthesized compounds with B-Raf enzyme.

Keywords

Antitumor; B-Raf; Cell cycle analysis; Molecular modeling; Pyridazinone.

1. Introduction

Cancer ranks high as a major cause of mortality worldwide.¹ Many Kinases are involved in signalling transduction pathways inside the cancer cells so that, these kinases are considered as good therapeutic targets for the discovery of new antitumor agents.^{2–5} B-Raf protein (Ser/Thr kinase) plays an important role in activating RAS–RAF–MEK–ERK signalling pathway and promoting normal cell development.⁶ B-Raf kinase is mutated in approximately 7% of all human cancer cells and the most common oncogenic mutation is V600E which is found in 90% of all B-Raf mutated cancer cells and

involves a substitution of valine by glutamic acid at codon 600.⁷ The deregulation of normal B-Raf signalling pathway leads to its over expression in different types of cancers; including colorectal (15%),⁸⁻¹⁰ hepatocellular (14%),^{10,11} mammary gland (10%),¹² melanoma (60%)^{10,13} and prostate cancer (10%).⁸ Several Raf inhibitors have been approved by FDA as anticancer drugs such as sorafenib,¹⁰ dabrafenib¹³ and vemurafenib¹⁴, while others are still under clinical trials such as WO2011068187¹⁵ (Figure 1).

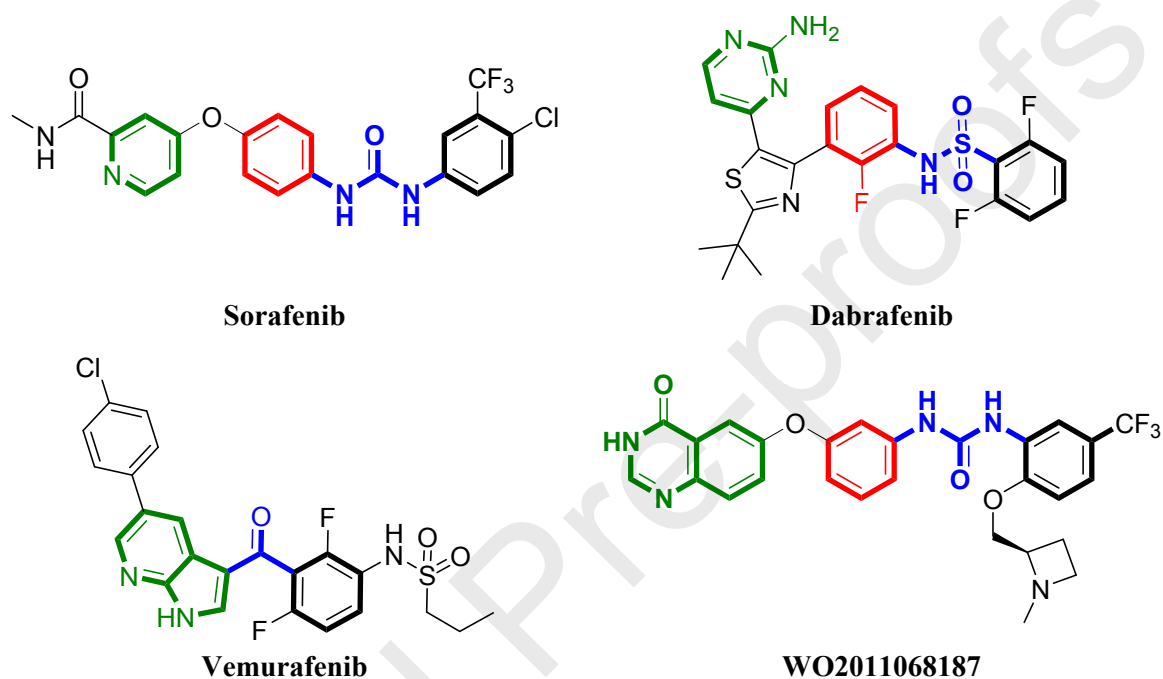


Figure 1: Reported Raf inhibitors.

2. Rational design

The study of the molecular modeling analysis of the crystal structure of B-Raf kinase with sorafenib (PDB code: 1UWJ)¹⁶ concluded common pharmacophoric features which are responsible for the good activity of B-Raf inhibitors. These features can be summarized as i) hetero aromatic ring that binds to the ATP pocket *via* hydrogen bonds which is necessary for high-binding affinity with the hinge region, mostly with Cys 531, ii) cyclic or non-cyclic linker, responsible for extending the molecule within the binding site, iii) a hydrogen bond network moiety which interacts with Asp 593 and/or Glu 500 residues at the DFG motif, iv) a lipophilic terminal which consists of a moiety that occupies the allosteric hydrophobic pocket that is formed between the DFG motif and the catalytic loop^{17, 18} (Figure 2).

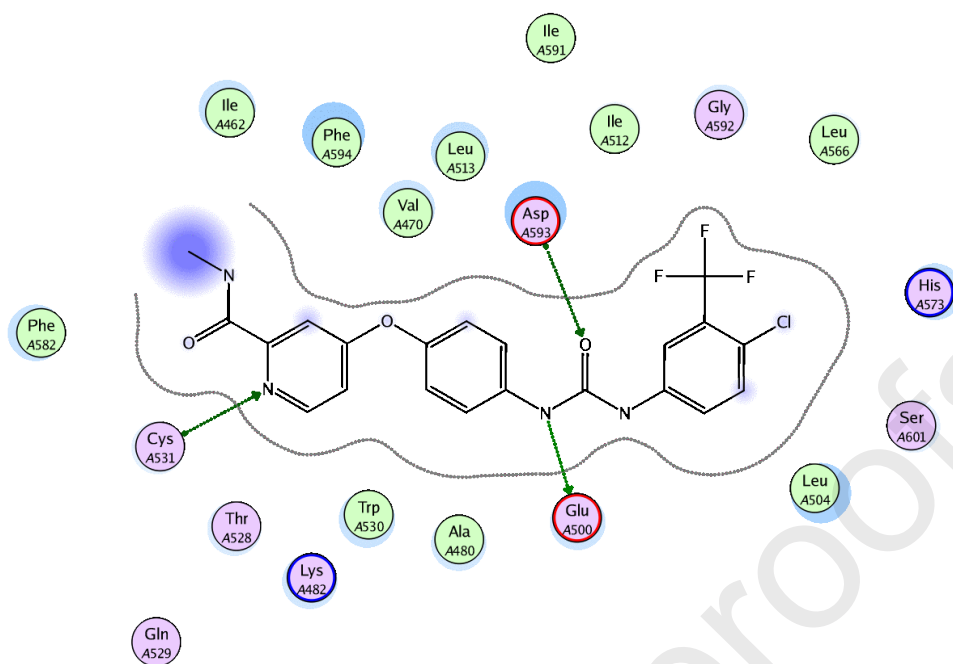


Figure 2: 2D interaction of the co-crystallized sorafenib inside the active site of B-Raf (PDB code: 1UWJ).¹⁶

The presence of nitrogenous heterocyclic moieties in the structure of the anticancer agents became essential to have potent activity such as pyridine, pyrimidine and pyridazine rings which are present in sorafenib, dabrafenib and vatalanib, respectively.¹⁹ While the presence of hydrogen bond network moiety in the skeleton of various anticancer agents plays an important role in improving their inhibitory activity against several types of kinases; this moiety may be urea as in sorafenib, heterocyclic ring as in vatalanib and encorafenib¹⁴ or imino group as in azastilben isoster **I**²⁰ (Figure 3).

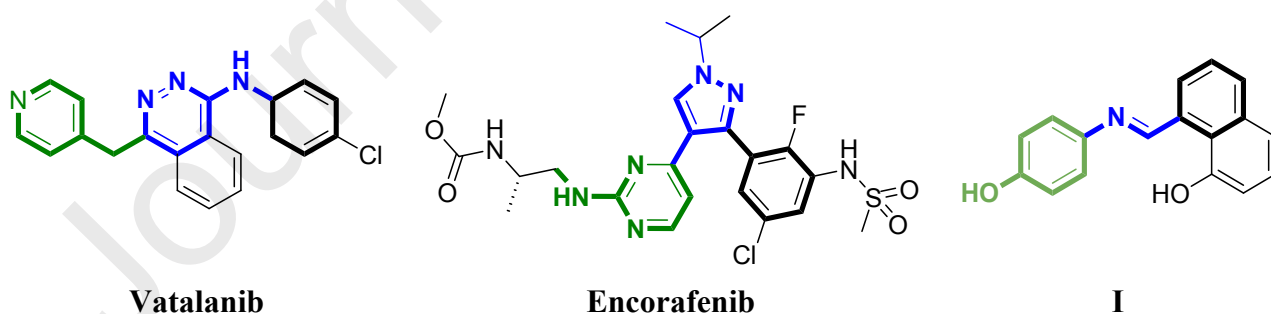


Figure 3: Reported antitumor agents.

Sorafenib was developed initially as an inhibitor for Raf kinase, but its efficacy in renal and hepatocellular cancer was later attributed to inhibition of VEGFR2, PDGFR and other targets.²¹ Later on, it faces a drug resistance,²² therefore we explored the structural modifications of sorafenib with the goal of optimizing its B-Raf kinase inhibition and/or anti-cancer activity.

As shown in figure 4, our target compounds were designed based on the structure of the lead compound; sorafenib; through computer-based design approach by incorporating different types of hydrogen bond network linkers at the center with phenyl pyridazinone scaffold from one end, and different hydrophobic moieties from the opposite end. The pyridazinone ring on the target series mimics the distal pyridine-carboxamide moiety of sorafenib. Also, the imino, triazole and (thio) urea moieties in the central core of the designed series mimic the urea moiety of sorafenib as hydrogen bond network linkers, likewise, the hydrophobic terminal in the target compounds and sorafenib. This optimization aims to give new derivatives which might be good B-Raf inhibitors with anticancer activity against a broad panel of cancer cell.

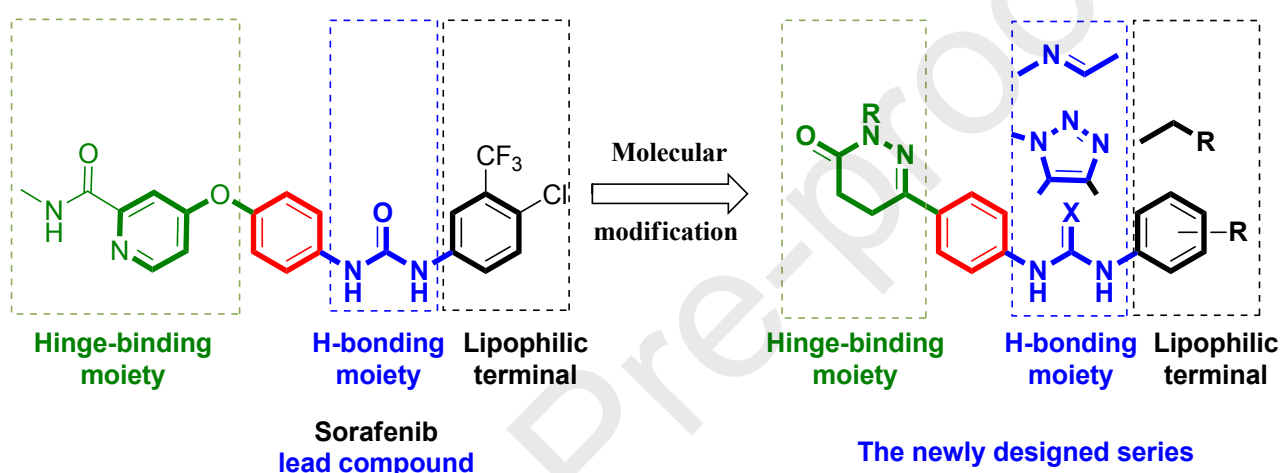
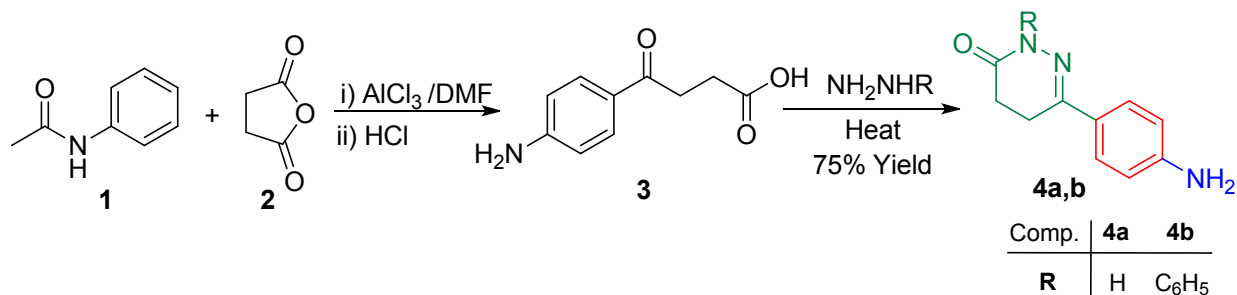


Figure 4: Rational design of the newly synthesized compounds.

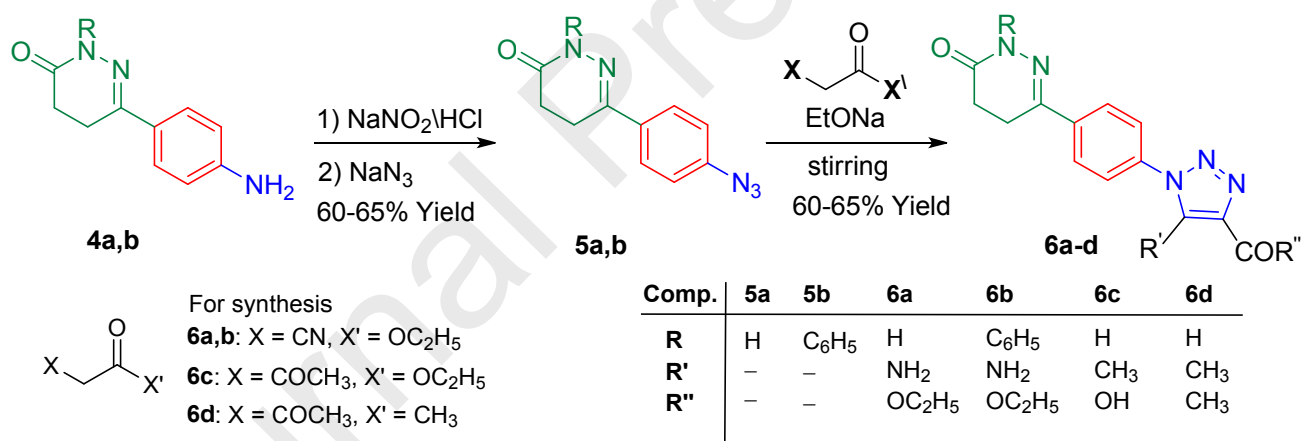
3. Results and discussion

3.1. Chemistry

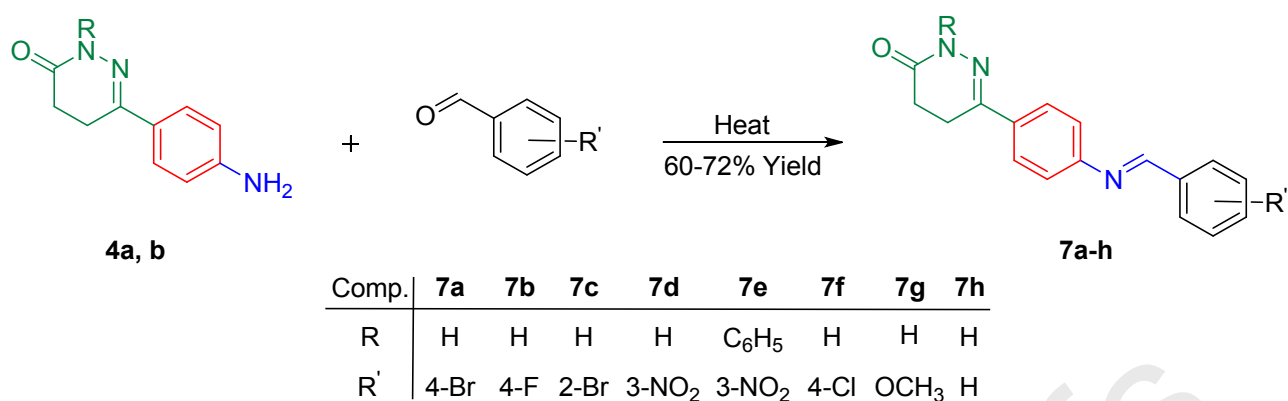
The designed target compounds were prepared as outlined in schemes 1-4. The structures of the target compounds were established based on elemental analysis, IR, $^1\text{H-NMR}$, $^{13}\text{C-NMR}$ and MS data. As shown in scheme 1, the preparation of pyridazinone derivatives **4a**²³ and **4b**, which are the key intermediates for the synthesis of our target compounds, was achieved *via* Friedel-Craft acylation^{24,25} of acetanilide (**1**) with succinic anhydride (**2**) in the presence of anhydrous AlCl_3 as a Lewis acid in DMF as a solvent, which was followed by acidic hydrolysis to give the corresponding γ -keto acid,²⁶⁻²⁹ as free amino derivative **3**. This intermediate was cyclized with hydrazine hydrate or phenyl hydrazine to afford the required pyridazinone derivatives **4a** and **4b**.

Scheme 1: Synthesis of the key intermediates **4a,b**.

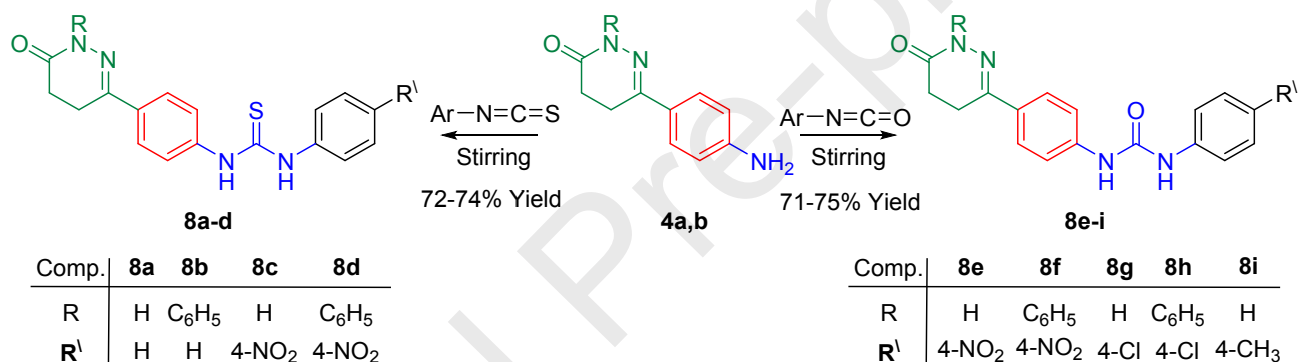
The azido derivatives **5a,b** were obtained through diazotization of amino compounds **4a,b** by sodium nitrite and HCl, followed by reacting with sodium azide.³⁰ The IR spectra of the compounds **5a,b** showed the disappearance of the absorption band at 3300-3400 cm⁻¹ of NH₂ group and the appearance of a new absorption band at 2136-2143 cm⁻¹ of N₃ group. The triazolo derivatives **6a-d** were obtained through 1,3-dipolar cycloaddition reaction between **5a** or **5b** and different active methylene-containing compounds such as ethyl cyanoacetate, ethyl acetoacetate and acetyl acetone.³¹ It is worthy to mention that compound **6c** was obtained as carboxylic acid derivatives due to the hydrolysis of the ester group during the course of the reaction (Scheme 2).

Scheme 2: Synthesis of the designed triazole derivatives **6a-d**.

The Schiff base³² series **7a-h** was afforded by reacting **4a** or **4b** with different aromatic aldehydes. The ¹H-NMR spectra of compounds **7a-h** showed a signal in the range of 8.55-8.88 ppm characteristic for the (=Ar-H) proton.

Scheme 3: Synthesis of the designed Schiff base derivatives **7a-h**.

Reaction of aryl iso(thio)cyanate derivatives with compounds **4a,b** afforded the diphenylurea (or thiourea) derivatives **8a-i**.³³ The ¹H-NMR spectra of compounds **8a-i** showed two adjacent signals in the range of 8.60-10.48 ppm indicating the presence of (NHCONH) and (NHCSNH) protons.

Scheme 4: Synthesis of the designed (thio)urea derivatives **8a-i**.

The ¹H-NMR spectra of the all synthesized compounds showed a signal in the range of 10.79-10.98 ppm that have disappeared with the blocking of the amide nitrogen in the pyridazine ring indicating the presence of (-CONH) proton, in addition to two triplet signals at the range of 2.41-2.74 and 2.91-3.22 ppm characterizing the presence of (CH₂-CH₂) protons of the pyridazine ring.

3.2. Biological evaluation

3.2.1. In vitro cytotoxic evaluation

MTT procedure was used to evaluate the antitumor activity of the synthesized compounds **4b-8i** against five human tumor cell lines, using sorafenib as a reference drug. A pair of models was selected based on B-Raf expression; where four cell lines represented over-expressed mutated B-Raf; including colon carcinoma (HCT-116),⁸ hepatocellular carcinoma (HEPG-2),¹⁰ mammary gland (MCF-7)¹² and human prostate cancer (PC-3),⁸ while the fifth one; human cervical carcinoma (Hela); was selected as

a model which lacks an over-expression of mutated B-Raf.³⁴ Biological data (Table 1), revealed that nine compounds **6a**, **6c**, **7f-h** and **8a-d** exhibited the highest antitumor activities with IC₅₀ range of 7.50–19.07 μ M. Compound **8b** was the highest cytotoxic agent against all the tested cell lines and showed potent activity against PC-3 cell line (IC₅₀ 7.83 μ M) in comparison to sorafenib (IC₅₀ 11.53 μ M). While, compound **7h** showed high cytotoxicity against HEPG-2 cell line with IC₅₀ equal to 8.71 μ M when compared with sorafenib (IC₅₀ 9.18 μ M). Compounds **7f-h** were active against HEPG-2, HCT-116 and MCF-7 rather than Hela and PC-3. Compound **6a** was active against all the tested cell lines, while compound **6c** was active mainly against HCT-116 and Hela cell lines. Compounds **4b**, **5a**, **5b**, **6b**, **6d**, **7a-c** and **8e** showed moderate cytotoxic activity, while compounds **7d**, **8h** and **8i** were the weakest. Unfortunately, compounds **7e**, **8f** and **8g** were non cytotoxic.

Table 1. *In vitro* cytotoxicity of the synthesized compounds and sorafenib.

Compound	IC ₅₀ μ M				
	HEPG2	MCF-7	PC3	HCT-116	Hela
4b	74.08 \pm 3.80	39.04 \pm 2.60	59.76 \pm 3.70	81.52 \pm 4.30	60.64 \pm 3.40
5a	31.11 \pm 2.20	19.68 \pm 1.90	40.81 \pm 2.70	25.37 \pm 2.70	38.43 \pm 2.50
5b	24.83 \pm 1.90	28.94 \pm 2.00	49.60 \pm 3.10	20.78 \pm 1.80	41.86 \pm 2.70
6a	10.57 \pm 1.00	9.87 \pm 0.80	12.83 \pm 1.20	7.50 \pm 0.60	11.63 \pm 1.00
6b	29.11 \pm 2.00	54.02 \pm 3.50	42.05 \pm 3.00	32.41 \pm 2.20	40.57 \pm 2.60
6c	18.79 \pm 1.50	14.56 \pm 1.30	25.61 \pm 1.70	11.19 \pm 1.10	13.06 \pm 1.20
6d	43.16 \pm 2.70	36.23 \pm 2.40	63.94 \pm 3.8	52.38 \pm 3.40	27.18 \pm 1.90
7a	69.55 \pm 3.50	45.12 \pm 2.70	62.04 \pm 3.80	76.82 \pm 4.00	64.80 \pm 3.80
7b	53.81 \pm 3.10	73.08 \pm 3.90	90.18 \pm 5.10	48.17 \pm 3.40	82.75 \pm 4.70
7c	50.97 \pm 2.90	34.81 \pm 2.30	54.86 \pm 3.50	43.79 \pm 3.20	58.13 \pm 3.00
7d	83.10 \pm 4.00	59.16 \pm 3.30	77.23 \pm 4.00	88.14 \pm 4.50	75.13 \pm 3.90
7e	68.73 \pm 3.60	93.72 \pm 5.20	>100	72.80 \pm 3.80	>100
7f	13.95 \pm 1.20	16.71 \pm 1.50	33.42 \pm 2.30	14.91 \pm 1.40	27.38 \pm 2.00
7g	9.78 \pm 1.00	18.52 \pm 1.80	29.85 \pm 2.30	13.78 \pm 1.20	32.84 \pm 2.30
7h	8.71 \pm 0.60	15.83 \pm 1.50	28.03 \pm 1.80	10.36 \pm 0.90	23.91 \pm 1.90
8a	36.02 \pm 2.40	7.59 \pm 0.40	8.96 \pm 0.70	26.38 \pm 2.50	12.60 \pm 1.10
8b	9.46 \pm 0.80	8.26 \pm 0.60	7.83 \pm 0.50	11.35 \pm 1.10	15.02 \pm 1.30
8c	17.86 \pm 1.50	13.25 \pm 1.30	27.74 \pm 1.40	19.07 \pm 1.60	21.78 \pm 1.50
8d	29.50 \pm 2.10	12.13 \pm 1.10	11.78 \pm 0.90	22.36 \pm 1.90	17.31 \pm 1.60
8e	42.34 \pm 2.60	30.40 \pm 2.20	51.20 \pm 3.20	37.56 \pm 2.90	46.78 \pm 2.80
8f	>100	87.26 \pm 4.70	>100	>100	91.42 \pm 5.30
8g	>100	80.34 \pm 4.30	>100	95.43 \pm 5.40	86.42 \pm 4.60
8h	94.23 \pm 4.60	52.73 \pm 2.90	86.52 \pm 4.80	89.25 \pm 4.70	71.49 \pm 3.70
8i	61.72 \pm 3.40	65.65 \pm 3.70	82.33 \pm 4.40	70.12 \pm 3.70	79.22 \pm 4.20
Sorafenib	9.18 \pm 0.60	7.26 \pm 0.30	11.53 \pm 0.90	5.47 \pm 0.30	8.04 \pm 0.50

3.2.2. B-Raf inhibition assay

The most active compounds **6a**, **6c**, **7f-h** and **8a-d** were selected for further enzyme inhibition screening against B-Raf (V600E).^{35,36} Compounds **8a**, **8b** and **8d** showed the highest affinity to B-Raf with IC₅₀ values range of 24.97-35.59 nM more than that of sorafenib (IC₅₀ 44.05 nM), whereas compound **8c** showed IC₅₀ value of 44.60 nM; nearly similar to that of sorafenib. On the other hand, compounds **7f-h** showed lower affinity to B-Raf with IC₅₀ value range of 70.65-84.14 nM, while compounds **6a** and **6c** showed the weakest inhibitory activity (Table 2).

Table 2. B-Raf enzyme inhibitory activity for compounds **6a**, **6c**, **7f-h** and **8a-d**.

Compound	6a	6c	7f	7g	7h
B-Raf IC ₅₀ (nM)	110.23±0.04	120.92±0.04	74.84±0.03	70.65±0.01	84.14±0.03
Compound	8a	8b	8c	8d	Sorafenib
B-Raf IC ₅₀ (nM)	30.83±0.01	24.97±0.01	44.60±0.007	35.59±0.005	44.05±0.02

3.2.3. Cell cycle analysis

Results of the cytotoxicity and the B-Raf inhibitory activity encouraged us to further evaluate the effect of compound **8b** on cell cycle distribution in MCF-7 cancer cell line. MCF-7 cells were incubated with compound **8b** at a concentration of 3 µg/ml for 24 h, stained with propidium iodide (PI) and analyzed by flow cytometry (FCM) using BD FACS caliber reader³⁷ (Figure 5).

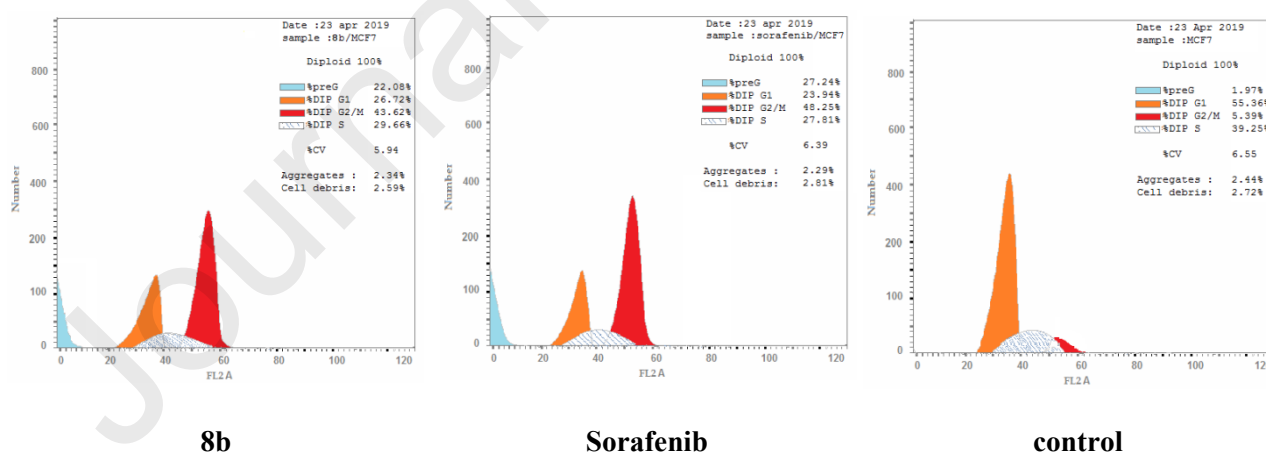


Figure 5: Effect of compound **8b** and sorafenib on the cell cycle distribution of MCF-7 cell line.

Table 3. Effect of **8b** and sorafenib on the cell cycle distribution of MCF-7 cell line.

Compound	Cell cycle distribution (%)			
	G0-G1	S	G2-M	Pre-G1
8b	26.72	29.66	43.62	22.08
Sorafenib	23.94	27.81	48.25	27.42
Control	55.36	39.25	5.39	1.97

Quantification of the results assessed that compound **8b** not only arrested MCF-7 cells in G2-M phase of the cell cycle at 24 h by 43.62% (Table 3); but it further caused induced block in G0-G1 phase by 26.72% as compared to that of sorafenib 23.94 % (Figure 6).

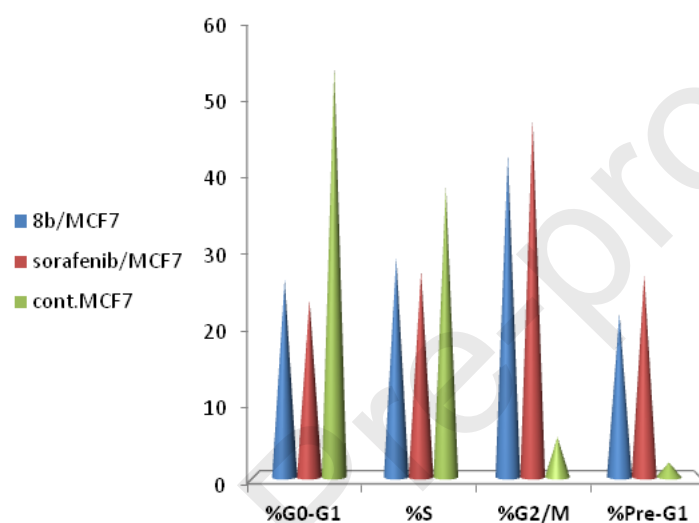


Figure 6: Effect of **8b** and sorafenib on the cell phases of MCF-7 cell line.

3.3.4. Detection of apoptosis

By analysing the data from histograms shown in figure 7, it was concluded that compound **8b** induced an early apoptotic effect 5.33% in MCF-7 cells after 24 h, beside a late apoptotic induction 15.03% nearly similar to sorafenib (15.78 %).

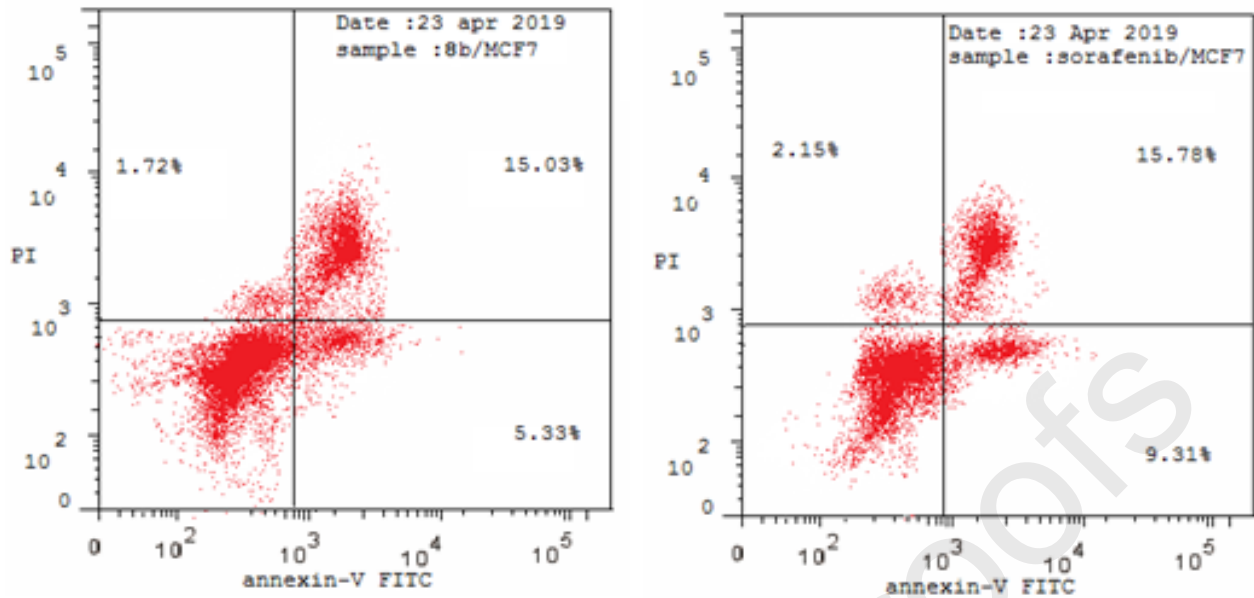
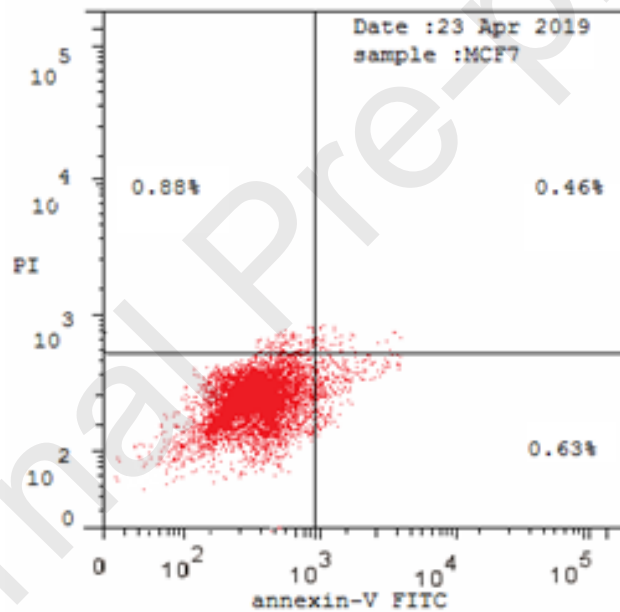
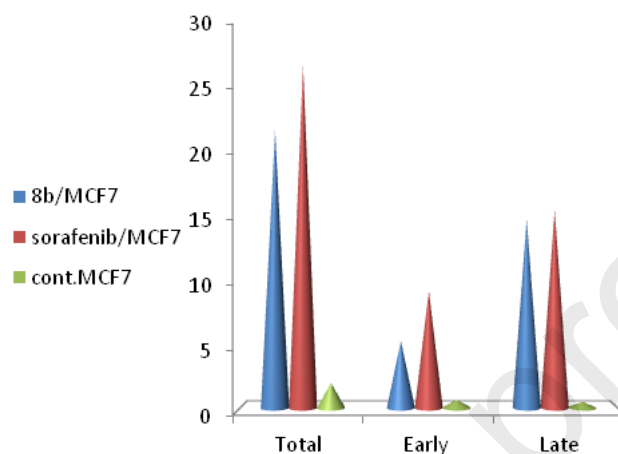
**8b****Sorafenib****Control**

Figure 7: Apoptosis induced by **8b** and sorafenib on MCF-7 cell line.

The total apoptosis (Figure 8) was determined by measuring the percent of cells stalled in the pre-G1 peak. It was estimated after 24 h exposure to be 22.08 and 27.24% for **8b** and sorafenib, respectively compared to the untreated MCF-7 cells 1.97% (Table 4).

Table 4. Apoptosis induced by **8b** and sorafenib on MCF-7.

Compound	Apoptosis			Necrosis
	Total	Early	Late	
8b	22.08	5.33	15.03	1.72
Sorafenib	27.24	9.31	15.78	2.15
Control	1.97	0.63	0.46	0.88

Figure 8. Early, late and total apoptosis induced by **8b** in comparison to sorafenib.

3.3. Molecular modeling

In this modeling study, we carried out the docking simulation using molecular operating environment software package (MOE 2013.08)³⁸⁻⁴⁰ in the binding site of B-Raf kinase⁴¹⁻⁴⁶ crystal structure with the active ligand sorafenib which was retrieved from the Protein Data Bank (PDB) at the Research Collaboratory for Structural Bioinformatics (RCSB, <http://www.rcsb.org>) (PDB code: 1UWJ).¹⁶ Careful analysis revealed that the binding cavity is surrounded by the catalytic amino acids Ala 480, Asp 593, Cys 531, Glu 500, Gly 595, His 573, Ile 512, Ile 571, Leu 504, Leu 513, Lys 482, Lys 566, Phe 582, Phe 594, Ser 601, Thr 528, Trp 530 and Val 503. As shown in figure 2, sorafenib forms three hydrogen bonds; one of them exists between the pyridyl nitrogen and Cys 531, while the other two hydrogen bonds are formed between the urea spacer and Glu 500 and Asp 593 amino acid residues with energy of interaction -8.32 kcal/mol. It is observed that compound **8b** (from thiourea series), which gave the best B-Raf inhibitory activity, forms three hydrogen bonds; two of them are formed between the thiourea nitrogens and the essential conserved amino acid residue Glu 500, while the third bond is formed between the amide oxygen of pyridazine ring and Cys 531 with energy of interaction -8.67 kcal/mol (Figure 9). Such binding mode is similar to that of sorafenib and well explains the high inhibitory activity of **8b** against B-Raf.

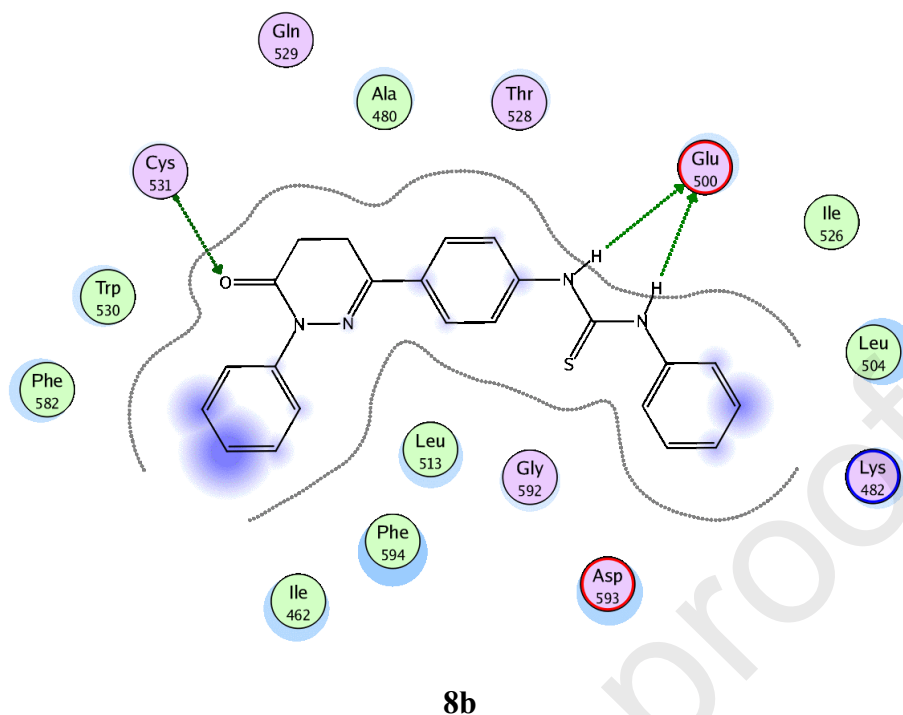


Figure 9: 2D interaction of compound **8b** with the binding site of B-Raf (PDB code: 1UWJ).

In a similar way, the synthesized compounds were found to form various interactions with the catalytic amino acid residues in the active binding site with energy of interaction ranging from -6.60 to -8.55 kcal/mol. As shown in figure 10, compounds **6a** (from triazole series) and **7g** (from imine series) retained the binding with the conserved amino acid residue Asp 593, while **7g** lacks the binding with Glu 500 in contrast to compound **6a**. Both compounds **6a** and **7g** interact with Thr 528 through the nitrogen atom of the pyridazine ring, while the oxygen of the methoxy group in **7g** binds to Ser 601 residue. The superior activity of **7g** over **6a** could be explained by the presence of the lipophilic phenyl terminal in **7g**, which lies in the hydrophobic pocket of the enzyme's active site, and the presence of the hydrophilic ester terminal in **6a** instead of the essential aromatic moiety.

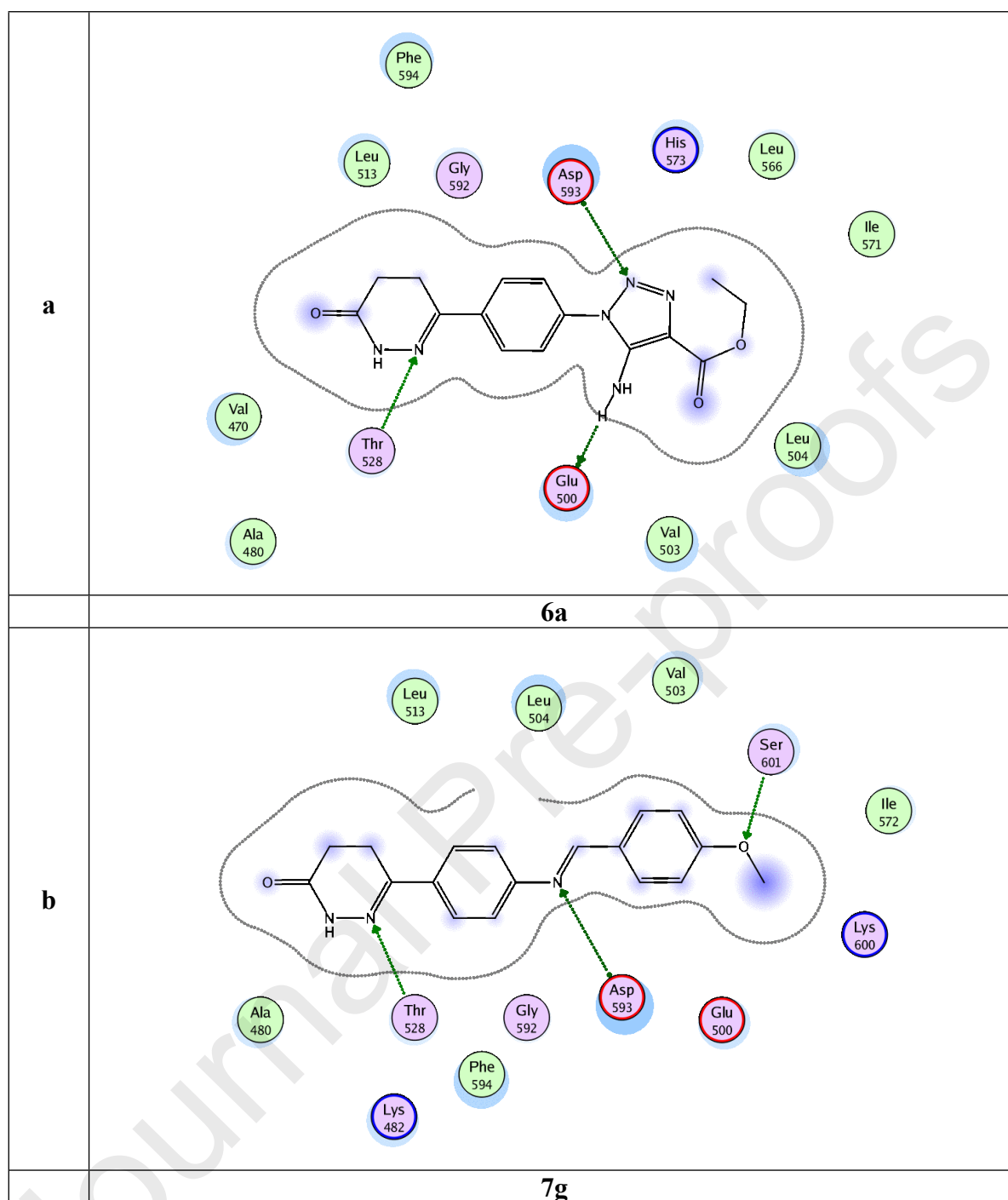


Figure 10: 2D interaction of compounds **6a** and **7g** within the binding site of B-Raf (PDB code: 1UWJ).

3.4. ADMET properties and Lipinski's rule of five

Lipinski's rule of five^{47, 48} is a principle used to evaluate drug likeness. All calculated descriptors were obtained using the molecular operating environment software package (MOE 2013.08)⁴⁹. The obtained results (Table 5) revealed that compounds **6a**, **7g** and **8b** along with sorafenib fulfil Lipinski's rule

with no violations. The calculated lipophilicity of **6a**, **7g**, **8b** and sorafenib proposed a good bioavailability with topological surface area lower than 140\AA^2 .

Table 5. ADMET properties prediction parameters of **6a**, **7g**, **8b** and sorafenib.

Compound	Mwt/g	TPSA/ \AA^2	LogP	nHBA	nHBD	nV
6a	328.33	124.49	1.31	6	2	0
7g	307.35	63.05	2.59	4	1	0
8b	400.50	88.82	3.83	2	2	0
Sorafenib	464.83	92.35	2.91	7	3	0

Mwt: molecular weight, TPSA: topological surface area, LogP: calculated lipophilicity, nHBA: number of hydrogen bond acceptors, nHBD: number of hydrogen bond donors, nV: number of violations of Lipinski's rules

3.5. SAR study

The results of the B-Raf inhibition assays (Table 2) revealed that compounds **6a** and **6c** from the triazole series (R = H) showed the least inhibitory activity against B-Raf where compounds **6a** and **6c** represented an IC_{50} value of about 3-folds than sorafenib. While, compounds **7f**, **7g** and **7h** from the imine series (R = H) showed better B-Raf inhibitory effect than triazole series with IC_{50} value of about 2-folds than sorafenib. These results indicate the importance of the lipophilic aromatic ring in the right terminal of the linker (N=CHAr) in order to boost the activity. Interestingly, thiourea series (**8a**, **8b**, **8c** and **8d**) exhibited the best inhibitory activity among other series indicating that the thiourea linker is essential for B-Raf affinity. Comparison between compounds **8a**, **8b**, **8c** and **8d** revealed that the *N*-phenyl substitution on the pyridazinone ring leads to improve the inhibitory activity rather than the non substituted analogues. Moreover, *p*-nitro substitution on the phenyl ring (right lipophilic terminal) lowers the activity in comparison to the unsubstituted analogue. Docking study assessed the biological results, since it showed that the thiourea-containing derivatives form five hydrogen bonds with the active site; with energies of interaction ranging from -8.85 to -10.99 kcal/mol. These interactions increase the ligand-receptor affinity and stabilize the ligand-receptor complex, resulting in the enhanced enzymatic activity of the whole series.

4. Conclusion

New series of phenyl dihydropyridazinone derivatives **4b–8i** have been designed, synthesized and evaluated for their *in vitro* cytotoxicity against different cell lines. Among the most promising cytotoxic agents, compounds **6a**, **6c**, **7f–h** and **8a–d**, were selected to evaluate their B-Raf inhibitory effect. Thiourea series including compounds **8a**, **8b**, and **8d** showed the highest affinity to B-Raf with IC_{50} values ranging from 24.97 to 35.59 nM when compared to sorafenib (IC_{50} 44.05 nM). The results

were consistent with the docking simulation. Compound **8b**, which exhibited the best cytotoxicity and B-Raf affinity, was induced early and late apoptosis, and showed cell cycle arrest at G₂-M phase. The results of molecular modeling and biological screening reveal that the structural modification of sorafenib as a lead structure affected the activity in a predictable manner.

5. Experimental

5.1. Chemistry

Melting points (°C) were recorded using Stuart SMP10 melting point apparatus and are uncorrected. IR spectra were recorded on a Thermo Fisher Scientific, Nicolet Is10 FT-IR spectrometer (cm^{-1}) using KBr disk at the Faculty of Pharmacy, Mansoura University, Egypt. NMR spectra were recorded on Bruker Avance NMR spectrometer (400 MHz) in DMSO-*d*₆ at Georgia State University, Atlanta, GA (¹H-NMR for compounds **4b**, **5b** and **7a-h**); Bruker Avance NMR spectrometer (400 MHz) in DMSO-*d*₆ at Faculty of Pharmacy, Mansoura University, Egypt (¹H and ¹³C-NMR for compounds **6a** and **6c-d**) and on Jeol ECA NMR spectrometer (500 MHz) in DMSO-*d*₆ at Faculty of Science Mansoura University (¹H and ¹³C-NMR for compounds **6b** and **8a-i**; ¹³C-NMR of compounds **7a-h**). The chemical shifts in ppm are expressed in δ units, using TMS as an internal standard and coupling constants in Hz. Mass spectrum analyses were performed on Thermo Scientific ISQ-LT quadrupole GC-MS at the regional centre for mycology and biotechnology (RCMB) Al-Azhar University. Elemental analysis was performed at micro analytical Unit, Cairo University and the results were within the valid range. Reaction times were monitored on TLC plates (F₂₅₄, Merck) using chloroform/methanol (9:1) as elution solvent and the spots were visualized by U.V. (366, 245 nm). Compound **4a** was prepared according to the procedure described in the literature.⁵⁰

5.1.1. Synthesis of 6-(4-aminophenyl)-2-phenyl-4,5-dihydropyridazin-3(2H)-one (**4b**).

A mixture of 4-(4-aminophenyl)-4-oxobutanoic acid (**3**) (1.930 g, 10 mmol) and phenyl hydrazine (1.080 g, 10 mmol) in absolute ethanol (10 ml) was heated under reflux for 8 h and then cooled. The resultant precipitate was collected by filtration, dried, and crystallized from ethanol to give **4b**:

Yield (1.99 g, 75%); m.p. 135-137 °C; IR (KBr) cm^{-1} , 3410, 3360 (NH₂), 3234 (CH), 1668 (CO); ¹H-NMR (400MHz, DMSO-*d*₆): δ 2.64 (t, *J* = 7.7 Hz, 2H, CH₂), 3.01 (t, *J* = 7.7 Hz, 2H, CH₂), 5.59 (s, 2H, NH₂), 6.59 (d, *J* = 8.0 Hz, 2H, Ar-H), 7.25 (dd, *J* = 7.2, 7.2 Hz, 1H, Ar-H), 7.41 (dd, *J* = 7.5, 7.5 Hz, 2H, Ar-H), 7.54-7.56 (m, 4H, Ar-H).

5.1.2. General method for synthesis of 6-(4-azidophenyl)-4,5-dihydropyridazin-3(2H)-one derivatives (**5a,b**).

Compound **4a** or **4b** (10 mmol) was dissolved in hydrochloric acid (17%, 20 mL) at room temperature. The solution was cooled to 0 °C using ice bath; and sodium nitrite (0.104 g, 15mmol) was added in small portions with stirring, then sodium azide (0.098 g, 15 mmol) was slowly added portion wise. The reaction mixture was then stirred for additional 2 h at room temperature. The separated solid was filtered, dried, and crystallized from ethanol to give the titled azido compounds **5a, b**.

6-(4-Azidophenyl)-4,5-dihydropyridazin-3(2H)-one (5a).

Yield (1.29 g, 60%); m.p. 96-98 °C; IR (KBr) cm^{-1} , 3448 (NH), 2918 (CH), 2143 (N_3), 1678 (CO); $^1\text{H-NMR}$ (400 MHz, $\text{DMSO-}d_6$): δ 2.57 (t, $J = 6.2$ Hz, 2H, CH_2), 3.22 (t, $J = 6.2$ Hz, 2H, CH_2), 7.24 (d, $J = 8.5$ Hz, 2H, Ar-H), 8.01 (d, $J = 8.5$ Hz, 2H, Ar-H), 12.16 (s, 1H, NH).

6-(4-Azidophenyl)-2-phenyl-4,5-dihydropyridazin-3(2H)-one (5b).

Yield (1.89 g, 65%); m.p. 89-91 °C; IR (KBr) cm^{-1} , 2998 (CH), 2136 (N_3), 1676 (CO); $^1\text{H-NMR}$ (400 MHz, $\text{DMSO-}d_6$): δ 2.72 (t, $J = 7.8$ Hz, 2H, CH_2), 3.13 (t, $J = 7.8$ Hz, 2H, CH_2), 7.20 (d, $J = 8.6$ Hz, 2H, Ar-H), 7.28 (dd, $J = 7.3, 7.3$ Hz, 1H, Ar-H), 7.43 (dd, $J = 7.7, 7.7$ Hz, 2H, Ar-H), 7.53 (d, $J = 7.7$ Hz, 2H, Ar-H), 7.88 (d, $J = 8.6$ Hz, 2H, Ar-H).

5.1.3. General method for synthesis of 6-(4-triazolophenyl)-4,5-dihydropyridazin-3(2H)-one derivatives (6a-d).

The methylene-activated compound (ethyl cyanoacetate, ethyl acetoacetate or acetyl acetone) (15 mmol) was added to freshly prepared sodium ethoxide (15 mL) and stirred for 10 min at room temperature. The reaction mixture was treated with the azide **5a** or **5b** (10 mmol) and stirred at room temperature for 20 h. The obtained solid was filtered, dried, and recrystallized from ethanol to give the titled compounds **6a-d**.

Ethyl 5-amino-1-[4-(6-oxo-4,5-dihydropyridazin-3-yl)phenyl]-1H-1,2,3-triazole-4-carboxylate (6a).

For ethyl cyanoacetate with **5a**: Yield (2.07 g, 63%); m.p. 208-210 °C; IR (KBr) cm^{-1} , 3431, 3311 (NH_2), 3243 (NH), 2976 (CH), 1683 (CO), 1628 ($\text{C}=\text{N}$). $^1\text{H-NMR}$ (400 MHz, $\text{DMSO-}d_6$): δ 1.30 (t, $J = 7.1$ Hz, 3H, CH_3), 2.61 (t, $J = 6.1$ Hz, 2H, CH_2), 3.30 (t, $J = 6.1$ Hz, 2H, CH_2), 4.3 (q, $J = 7.1$ Hz, 2H, CH_2), 6.72 (s, 2H, NH_2), 7.75 (d, $J = 8.6$ Hz, 2H, Ar-H), 8.18 (d, $J = 8.6$ Hz, 2H, Ar-H), 12.23 (bs, 1H, NH). $^{13}\text{C-NMR}$ (100 MHz, $\text{DMSO-}d_6$): δ 14.88, 28.32, 33.79, 60.21, 119.74, (124.80, $\text{CH} \times 2$), (129.92, $\text{CH} \times 2$), 136.93, 138.58, 146.74, 162.13, 174.26, 198.31. EI-MS: (m/z, %): 328.15 (M^+ , 100), 329.10 (M^++1 , 18.95). Elemental analysis for $\text{C}_{15}\text{H}_{16}\text{N}_6\text{O}_3$ (328.33), calcd.: C, 54.87; H, 4.91; N, 25.60. Found: C, 54.91; H, 4.94; N, 25.61.

Ethyl 5-amino-1-[4-(6-oxo-1-phenyl-4,5-dihydropyridazin-3-yl)phenyl]-1H-1,2,3-triazole-4-carboxylate (6b).

For ethyl cyanoacetate with **5b**: Yield (2.47 g, 61%); m.p. 145-147 °C; IR (KBr) cm^{-1} , 3447 (NH_2), 2981 (CH), 1632 (CO). $^1\text{H-NMR}$ (500 MHz, $\text{DMSO-}d_6$): δ 1.31 (t, $J = 7.2$ Hz, 3H, CH_3), 2.78 (t, $J = 8.1$ Hz, 2H, CH_2), 3.21 (t, $J = 8.1$ Hz, 2H, CH_2), 4.30 (q, $J = 7.2$ Hz, 2H, CH_2), 6.64 (s, 2H, NH_2), 7.28 (dd, $J = 7.3, 7.3$ Hz, 1H, Ar-H), 7.45 (dd, $J = 7.5, 7.5$ Hz, 2H, Ar-H), 7.55 (d, $J = 7.5$ Hz, 2H, Ar-H), 7.65 (d, $J = 8.2$ Hz, 2H, Ar-H), 8.02 (d, $J = 8.2$ Hz, 2H, Ar-H). $^{13}\text{C-NMR}$ (125 MHz, $\text{DMSO-}d_6$): δ 14.42, 22.29, 27.28, 59.67, 119.18, (124.46, CH \times 2), (124.91, CH \times 2), 126.28, (127.46, CH \times 2), (128.16, CH \times 2), 135.37, 136.06, 141.32, 146.21, 150.82, 161.68, 165.25. EI-MS: (m/z, %): 404.09 (M^+ , 100), 405.19 (M^++1 , 24.55). Elemental analysis for $\text{C}_{21}\text{H}_{20}\text{N}_6\text{O}_3$ (404.43), calcd.: C, 62.37; H, 4.98; N, 20.78. Found: C, 62.34; H, 4.94; N, 20.79.

5-Methyl-1-[4-(6-oxo-4,5-dihydropyridazin-3-yl)phenyl]-1H-1,2,3-triazole-4-carboxylic acid (6c).

For ethyl acetoacetate with **5a**: Yield (1.80 g, 60%); m.p. 181-183 °C; IR (KBr) cm^{-1} , 3592 (OH), 3490 (NH), 2929 (CH), 1691 (CO), 1601 (C=N). $^1\text{H-NMR}$ (400 MHz, $\text{DMSO-}d_6$): δ 2.55 (s, 3H, CH_3), 2.61 (t, $J = 6.1$ Hz, 2H, CH_2), 3.32 (t, $J = 6.1$ Hz, 2H, CH_2), 7.81 (d, $J = 8.5$ Hz, 2H, Ar-H), 8.21 (d, $J = 8.5$ Hz, 2H, Ar-H), 12.44 (brs, 1H, NH). $^{13}\text{C-NMR}$ (100 MHz, $\text{DMSO-}d_6$): δ 10.28, 28.31, 33.85, (126.04, CH \times 2), (129.79, CH \times 2), 137.28, 137.63, 139.14, 139.70, 162.98, 174.27, 198.35; EI-MS: (m/z, %): 299.15 (M^+ , 100), 300.19 (M^++1 , 16.55). Elemental analysis for $\text{C}_{14}\text{H}_{13}\text{N}_5\text{O}_3$ (299.29), calcd.: C, 56.18; H, 4.38; N, 23.40. Found: C, 66.15; H, 4.34; N, 23.37.

6-[4-(4-Acetyl-5-methyl-1H-1,2,3-triazol-1-yl)phenyl]-4,5-dihydropyridazin-3(2H)-one (6d).

For acetyl acetone with **5a**: Yield (1.93 g, 65%); m.p. 155-157 °C; IR (KBr) cm^{-1} , 3449 (NH), 2911 (CH), 1686 (CO), 1604 (C=N). $^1\text{H-NMR}$ (400 MHz, $\text{DMSO-}d_6$): δ 2.56 (s, 3H, CH_3), 2.62 (t, $J = 6.4$ Hz, 2H, CH_2), 2.65 (s, 3H, CH_3), 3.34 (t, $J = 6.4$ Hz, 2H, CH_2), 7.81 (d, $J = 8.6$ Hz, 2H, Ar-H), 8.21 (d, $J = 8.6$ Hz, 2H, Ar-H). $^{13}\text{C-NMR}$ (100 MHz, $\text{DMSO-}d_6$): δ 10.26, 28.18, 28.31, 33.86, (126.04, CH \times 2), (129.81, CH \times 2), 137.73, 138.42, 138.83, 143.48, 174.27, 193.87, 198.36. EI-MS: (m/z, %): 297.10 (M^+ , 100), 298.19 (M^++1 , 17.45). Elemental analysis for $\text{C}_{15}\text{H}_{15}\text{N}_5\text{O}_2$ (297.32), calcd.: C, 60.60; H, 5.09; N, 23.56. Found: C, 60.65; H, 5.13; N, 23.59.

5.1.4. General method for synthesis of 6-[4-(substituted benzylidene)amino]phenyl]pyridazin-3(2H)-one (7a-h).

A mixture of compound **4a** or **4b** (10 mmol) and the appropriate aromatic aldehydes (10 mmol) was dissolved in absolute ethanol (15 mL) with few drops of glacial acetic acid; then stirred under reflux

for 8 h. After cooling, the obtained solid was filtered, washed with water, dried, and crystallized from ethanol to give the titled compounds **7a-h**.

6-{4-[(4-Bromobenzylidene)amino]phenyl}-4,5-dihydropyridazin-3(2H)-one (7a).

Yield (2.53 g, 71%); m.p. 262-264 °C; IR (KBr) cm^{-1} , 3193 (NH), 2938 (CH), 1682 (CO), 1608 (C=N). $^1\text{H-NMR}$ (400 MHz, $\text{DMSO-}d_6$): δ 2.48 (t, $J = 8.0$ Hz, 2H, CH_2), 2.97 (t, $J = 8.0$ Hz, 2H, CH_2), 7.33 (d, $J = 7.9$ Hz, 2H, Ar-H), 7.74 (d, $J = 7.9$ Hz, 2H, Ar-H), 7.80 (d, $J = 7.9$ Hz, 2H, Ar-H), 7.89 (d, $J = 7.9$ Hz, 2H, Ar-H), 8.68 (s, 1H, =CH-Ar), 10.95 (s, 1H, NH). $^{13}\text{C-NMR}$ (125 MHz, $\text{DMSO-}d_6$): δ 21.82, 25.99, (121.28, CH \times 2), 125.23, (126.67, CH \times 2), (130.57, CH \times 2), (131.95, CH \times 2), 133.85, 135.09, 148.96, 151.64, 160.03, 166.99. EI-MS: (m/z, %): 355.05 (M^+ , 100), 357.03 ($\text{M}^+ + 2$, 96.45). Elemental analysis for $\text{C}_{17}\text{H}_{14}\text{BrN}_3\text{O}$ (356.22), calcd.: C, 57.32; H, 3.96; N, 11.80. Found: C, 57.30; H, 3.92; N, 11.77.

6-{4-[(4-Fluorobenzylidene)amino]phenyl}-4,5-dihydropyridazin-3(2H)-one (7b).

Yield (1.87 g, 72%); m.p. 246-248 °C; IR (KBr) cm^{-1} , 3449 (NH), 2988 (CH), 1630 (CO), 1600 (C=N). $^1\text{H-NMR}$ (400 MHz, $\text{DMSO-}d_6$): δ 2.46 (t, $J = 8.0$ Hz, 2H, CH_2), 2.97 (t, $J = 8.0$ Hz, 2H, CH_2), 7.33 (d, $J = 8.2$ Hz, 2H, Ar-H), 7.39 (dd, $J = 8.6, 8.6$ Hz, 2H, Ar-H), 7.81 (d, $J = 8.2$ Hz, 2H, Ar-H), 8.02 (dd, $J = 5.9, 5.9$ Hz, 2H, Ar-H), 8.67 (s, 1H, =CH-Ar), 10.95 (s, 1H, NH). $^{13}\text{C-NMR}$ (100 MHz, $\text{DMSO-}d_6$): δ 22.30, 26.48, (121.77, CH \times 2), (127.15, CH \times 2), (129.51, CH \times 2), (130.88, CH \times 2), 134.32, 135.26, 136.70, 149.45, 152.14, 160.39, 167.48. EI-MS: (m/z, %): 295.15 (M^+ , 100), 296.10 ($\text{M}^+ + 1$, 19.45). Elemental analysis for $\text{C}_{17}\text{H}_{14}\text{FN}_3\text{O}$ (295.32), calcd.: C, 69.14; H, 4.78; N, 14.23. Found: C, 69.18; H, 4.80; N, 14.21.

6-{4-[(2-Bromobenzylidene)amino]phenyl}-4,5-dihydropyridazin-3(2H)-one (7c).

Yield (2.32 g, 65%); m.p. 163-165 °C; IR (KBr) cm^{-1} , 3293 (NH), 2968 (CH), 1680 (CO), 1613 (C=N). $^1\text{H-NMR}$ (400 MHz, $\text{DMSO-}d_6$): δ 2.45 (t, $J = 8.1$ Hz, 2H, CH_2), 2.98 (t, $J = 8.1$ Hz, 2H, CH_2), 7.34 (d, $J = 8.4$ Hz, 2H, Ar-H), 7.52 (dd, $J = 8.6, 8.6$ Hz, 2H, Ar-H), 7.77 (d, $J = 7.5$ Hz, 1H, Ar-H), 7.82 (d, $J = 8.4$ Hz, 2H, Ar-H), 8.81 (d, $J = 7.5$ Hz, 1H, Ar-H), 8.82 (s, 1H, =CH-Ar), 10.98 (s, 1H, NH). $^{13}\text{C-NMR}$ (100 MHz, $\text{DMSO-}d_6$): δ 22.29, 26.47, (121.94, CH \times 2), 123.35, 126.28, (127.18, CH \times 2), 131.03, 134.75, 135.15, 137.93, 148.67, 149.36, 151.55, 159.69, 167.48. EI-MS: (m/z, %): 355.15 (M^+ , 100), 357.09 ($\text{M}^+ + 2$, 96.65). Elemental analysis for $\text{C}_{17}\text{H}_{14}\text{BrN}_3\text{O}$ (356.22), calcd.: C, 57.32; H, 3.96; N, 11.80. Found: C, 57.36; H, 4.00; N, 11.77.

6-{4-[(3-Nitrobenzylidene)amino]phenyl}-4,5-dihydropyridazin-3(2H)-one (7d).

Yield (2.26 g, 70%); m.p. 220-222 °C; IR (KBr) cm^{-1} , 3211 (NH), 2945 (CH), 1679 (CO), 1610 (C=N). $^1\text{H-NMR}$ (400 MHz, $\text{DMSO-}d_6$): δ 2.46 (t, $J = 8.2$ Hz, 2H, CH_2), 2.99 (t, $J = 8.2$ Hz, 2H, CH_2), 7.38 (d, $J = 8.4$ Hz, 2H, Ar-H), 7.83–7.85 (m, 3H, Ar-H), 8.37 (dd, $J = 6.5, 6.5$ Hz, 2H, Ar-H), 8.75 (s, 1H, Ar-H), 8.68 (s, 1H, =CH-Ar), 10.79 (s, 1H, NH). $^{13}\text{C-NMR}$ (125 MHz, $\text{DMSO-}d_6$): δ 21.83, 25.99, (121.47, CH \times 2), 122.98, 125.83, (126.72, CH \times 2), 130.58, 134.30, 134.68, 137.48, 148.28, 148.91, 151.10, 159.27, 167.01. EI-MS: (m/z, %): 322.21 (M^+ , 100), 323.23 (M^++1 , 22.91). Elemental analysis for $\text{C}_{17}\text{H}_{14}\text{N}_4\text{O}_3$ (322.32), calcd.: C, 63.35; H, 4.38; N, 17.38. Found: C, 63.31; H, 4.42; N, 17.37.

6-{4-[(3-Nitrobenzylidene)amino]phenyl}-2-phenyl-4,5-dihydropyridazin-3(2H)-one (7e).

Yield (2.39 g, 60%); m.p. 211-213 °C; IR (KBr) cm^{-1} , 3063 (CH), 1679 (CO), 1630 (C=N). $^1\text{H-NMR}$ (400 MHz, $\text{DMSO-}d_6$): δ 2.75 (t, $J = 7.9$ Hz, 2H, CH_2), 3.17 (t, $J = 7.9$ Hz, 2H, CH_2), 7.27 (dd, $J = 7.2, 7.2$ Hz, 1H, Ar-H), 7.41–7.46 (m, 4H, Ar-H), 7.56 (d, $J = 7.9$ Hz, 2H, Ar-H), 7.83 (dd, $J = 7.9, 7.9$ Hz, 1H, Ar-H), 7.92 (d, $J = 8.0$ Hz, 2H, Ar-H), 8.38 (d, $J = 7.5$ Hz, 2H, Ar-H) 8.76 (s, 1H, Ar-H), 8.87 (s, 1H, =CH-Ar). $^{13}\text{C-NMR}$ (125 MHz, $\text{DMSO-}d_6$): δ 21.11, 25.83, (121.31, CH \times 2), (121.02, CH \times 2), 123.01, 125.95, (125.99, CH \times 2), (126.02, CH \times 2), 130.49, 131.49, 132.38, 134.02, 134.28, 136.33, 146.75, 148.99, 150.85, 158.31, 167.81. EI-MS: (m/z, %): 398.10 (M^+ , 100), 399.19 (M^++1 , 26.65). Elemental analysis for $\text{C}_{23}\text{H}_{18}\text{N}_4\text{O}_3$ (398.42), calcd.: C, 69.34; H, 4.55; N, 14.06. Found: C, 69.30; H, 4.51; N, 14.07.

6-{4-[(4-Chlorobenzylidene)amino]phenyl}-4,5-dihydropyridazin-3(2H)-one (7f).

Yield (2.18 g, 71%); m.p. 271-273 °C; IR (KBr) cm^{-1} , 3195 (NH), 2940 (CH), 1684 (CO), 1609 (C=N). $^1\text{H-NMR}$ (400 MHz, $\text{DMSO-}d_6$): δ 2.48 (t, $J = 8.1$ Hz, 2H, CH_2), 2.97 (t, $J = 8.1$ Hz, 2H, CH_2), 7.33 (d, $J = 8.1$ Hz, 2H, Ar-H), 7.60 (d, $J = 8.0$ Hz, 2H, Ar-H), 7.81 (d, $J = 8.1$ Hz, 2H, Ar-H), 7.97 (d, $J = 8.0$ Hz, 2H, Ar-H), 8.69 (s, 1H, =CH-Ar), 10.96 (s, 1H, NH). $^{13}\text{C-NMR}$ (125 MHz, $\text{DMSO-}d_6$): δ 21.82, 25.99, (121.28, CH \times 2), (126.66, CH \times 2), (129.02, CH \times 2), (130.40, CH \times 2), 133.83, 134.78, 136.23, 148.96, 151.65, 159.89, 166.99. EI-MS: (m/z, %): 311.09 (M^+ , 100), 313.19 (M^++2 , 33.65). Elemental analysis for $\text{C}_{17}\text{H}_{14}\text{ClN}_3\text{O}$ (311.77), calcd.: C, 65.49; H, 4.53; N, 13.48. Found: C, 65.55; H, 4.57; N, 13.50.

6-{4-[(4-Methoxybenzylidene)amino]phenyl}-4,5-dihydropyridazin-3(2H)-one (7g).

Yield (1.91 g, 62%); m.p. 211-213 °C; IR (KBr) cm^{-1} , 3208 (NH), 2931 (CH), 1679 (CO), 1622 (C=N). $^1\text{H-NMR}$ (400 MHz, $\text{DMSO-}d_6$): δ 2.45 (t, $J = 8.1$ Hz, 2H, CH_2), 2.97 (t, $J = 8.1$ Hz, 2H, CH_2), 3.85 (s, 3H, -OCH₃), 7.08 (d, $J = 8.4$ Hz, 2H, Ar-H), 7.28 (d, $J = 8.2$ Hz, 2H, Ar-H), 7.78 (d, $J = 8.2$ Hz,

2H, Ar-H), 7.90 (d, $J = 8.4$ Hz, 2H, Ar-H), 8.58 (s, 1H, =CH-Ar), 10.93 (s, 1H, NH). ^{13}C -NMR (100 MHz, DMSO- d_6): δ 22.29, 26.50, 55.91, (114.79, CH \times 2), (121.61, CH \times 2), (127.11, CH \times 2), 129.30, (131.12, CH \times 2), 133.65, 149.55, 152.86, 160.74, 162.54, 167.49. EI-MS: (m/z, %): 307.15 (M^+ , 100), 308.19 ($\text{M}^+ + 1$, 20.65). Elemental analysis for $\text{C}_{18}\text{H}_{17}\text{N}_3\text{O}_2$ (307.35), calcd.: C, 70.34; H, 5.58; N, 13.67. Found: C, 70.30; H, 5.57; N, 13.65.

6-[4-(Benzylideneamino)phenyl]-4,5-dihydropyridazin-3(2H)-one (7h).

Yield (1.66 g, 60%); m.p. 248-250 °C; IR (KBr) cm^{-1} , 3218 (NH), 2991 (CH), 1670 (CO), 1620 (C=N). ^1H -NMR (400 MHz, DMSO- d_6): δ 2.48 (t, $J = 7.9$ Hz, 2H, CH_2), 2.98 (t, $J = 7.9$ Hz, 2H, CH_2), 7.32 (d, $J = 8.0$ Hz, 2H, Ar-H), 7.46 – 7.55 (m, 3H, Ar-H), 7.44 (d, $J = 8.1$ Hz, 2H, Ar-H), 7.81 (d, $J = 8.0$ Hz, 2H, Ar-H), 8.68 (s, 1H, =CH-Ar), 10.98 (s, 1H, NH). ^{13}C -NMR (125 MHz, DMSO- d_6): δ 21.22, 25.19, (121.87, CH \times 2), (125.96, CH \times 2), (128.82, CH \times 2), (129.81, CH \times 2), 133.12, 134.15, 131.11, 148.56, 151.53, 160.01, 166.69. EI-MS: (m/z, %): 277.15 (M^+ , 100), 278.19 ($\text{M}^+ + 1$, 20.15). Elemental analysis for $\text{C}_{17}\text{H}_{15}\text{N}_3\text{O}$ (277.33), calcd.: C, 73.63; H, 5.45; N, 15.15. Found: C, 73.69; H, 5.50; N, 15.12.

5.1.5. General method for synthesis of 1-[4-(6-oxo-4,5-dihydropyridazin-3-yl)phenyl]-3-phenylurea (or thiourea) derivatives (8a-i).

A mixture of compound **4a** or **4b** (10 mmol) and the appropriate aryl iso(thio)cyanate derivative (10 mmol) was dissolved in THF (10 mL) and stirred at room temperature for 4h. The resultant precipitate was collected by filtration, dried, and recrystallized from THF to give the titled compounds **8a-i**.

1-[4-(6-Oxo-4,5-dihydropyridazin-3-yl)phenyl]-3-phenylthiourea (8a).

Yield (2.37 g, 73%); m.p. 220-222 °C; IR (KBr) cm^{-1} , 3227 (NH), 3058 (NH), 2977 (CH); 1673 (CO). ^1H -NMR (500 MHz, DMSO- d_6): δ 2.43 (t, $J = 8.2$ Hz, 2H, CH_2), 2.93 (t, $J = 8.2$ Hz, 2H, CH_2), 7.13 (dd, $J = 7.2, 7.2$ Hz, 1H, Ar-H), 7.32 (dd, $J = 7.8, 7.8$ Hz, 2H, Ar-H), 7.47 (d, $J = 7.8$ Hz, 2H, Ar-H), 7.56 (d, $J = 8.8$ Hz, 2H, Ar-H), 7.70 (d, $J = 8.8$ Hz, 2H, Ar-H), 9.90 (s, 1H, NH), 9.95 (s, 1H, NH), 10.89 (s, 1H, NH). ^{13}C -NMR (125 MHz, DMSO- d_6): δ 22.17, 27.11, (122.29, CH \times 2), (124.01, CH \times 2), 124.38, (124.49, CH \times 2), 125.97, (126.26, CH \times 2), 140.23, 141.10, 150.29, 164.59, 179.29. EI-MS: (m/z, %): 324.12 (M^+ , 100), 325.19 ($\text{M}^+ + 1$, 19.19). Elemental analysis for $\text{C}_{17}\text{H}_{16}\text{N}_4\text{OS}$ (324.40), calcd.: C, 62.94; H, 4.97; N, 17.27. Found: C, 62.98; H, 5.00; N, 17.25.

1-[4-(6-Oxo-1-phenyl-4,5-dihydropyridazin-3-yl)phenyl]-3-phenylthiourea (8b).

Yield (2.96 g, 74%); m.p. 208-210 °C; IR (KBr) cm^{-1} , 3230 (NH), 3056 (NH), 2971 (CH); 1671 (CO). $^1\text{H-NMR}$ (500 MHz, $\text{DMSO-}d_6$): δ 2.71 (t, $J = 8.1$ Hz, 2H, CH_2), 3.11 (t, $J = 8.1$ Hz, 2H, CH_2), 7.13 (dd, $J = 7.3, 7.3$ Hz, 1H, Ar-H), 7.27 (dd, $J = 7.4, 7.4$ Hz, 1H, Ar-H), 7.33 (dd, $J = 7.9, 7.9$ Hz, 2H, Ar-H), 7.42 (dd, $J = 7.9, 7.9$ Hz, 2H, Ar-H), 7.47 (d, $J = 7.7$ Hz, 2H, Ar-H), 7.54 (d, $J = 7.7$, 2H, Ar-H), 7.61 (d, $J = 8.4$ Hz, 2H, Ar-H), 7.78 (d, $J = 8.4$ Hz, 2H, Ar-H), 9.92 (s, 1H, NH), 9.99 (s, 1H, NH). $^{13}\text{C-NMR}$ (125 MHz, $\text{DMSO-}d_6$): δ 22.12, 27.43, (122.70, $\text{CH} \times 2$), (123.63, $\text{CH} \times 2$), 124.57, (124.82, $\text{CH} \times 2$), 126.07, (126.38, $\text{CH} \times 2$), (128.29, $\text{CH} \times 2$), (128.50, $\text{CH} \times 2$), 130.87, 139.30, 141.06, 141.44, 151.60, 165.30, 179.32. EI-MS: (m/z, %): 400.12 (M^+ , 100), 404.19 ($\text{M}^+ + 1$, 26.89). Elemental analysis for $\text{C}_{23}\text{H}_{20}\text{N}_4\text{OS}$ (400.50), calcd.: C, 68.98; H, 5.03; N, 13.99. Found: C, 68.95; H, 5.00; N, 13.95.

1-(4-Nitrophenyl)-3-[4-(6-oxo-4,5-dihydropyridazin-3-yl)phenyl]thiourea (8c).

Yield (2.66 g, 72%); m.p. 200-202 °C; IR (KBr) cm^{-1} , 3447 (NH), 3212 (NH), 3100 (NH), 2950 (CH), 1645 (CO). $^1\text{H-NMR}$ (500 MHz, $\text{DMSO-}d_6$): δ 2.43 (t, $J = 8.3$ Hz, 2H, CH_2), 2.93 (t, $J = 8.3$ Hz, 2H, CH_2), 7.57 (d, $J = 8.7$ Hz, 2H, Ar-H), 7.73 (d, $J = 8.7$ Hz, 2H, Ar-H), 7.81 (d, $J = 9.1$ Hz, 2H, Ar-H), 8.19 (d, $J = 9.1$ Hz, 2H, Ar-H), 10.41 (s, 1H, NH), 10.46 (s, 1H, NH), 10.91 (s, 1H, NH). $^{13}\text{C-NMR}$ (100 MHz, $\text{DMSO-}d_6$): δ 22.17, 26.53, (118.24, $\text{CH} \times 2$), (120.28, $\text{CH} \times 2$), 125.96, (126.89, $\text{CH} \times 2$), (129.13, $\text{CH} \times 2$), 129.91, 139.02, 141.09, 149.64, 152.72, 167.46. EI-MS: (m/z, %): 369.15 (M^+ , 100), 370.19 ($\text{M}^+ + 1$, 20.85). Elemental analysis for $\text{C}_{17}\text{H}_{15}\text{N}_5\text{O}_3\text{S}$ (369.40), calcd.: C, 55.28; H, 4.09; N, 18.96. Found: C, 55.33; H, 4.14; N, 18.95.

1-(4-Nitrophenyl)-3-[4-(6-oxo-1-phenyl-4,5-dihydropyridazin-3-yl)phenyl]thiourea (8d).

Yield (3.30 g, 74%); m.p. 213-215 °C; IR (KBr) cm^{-1} , 3333 (NH), 3207 (NH), 2987 (CH), 1631 (CO). $^1\text{H-NMR}$ (500 MHz, $\text{DMSO-}d_6$): δ 2.72 (t, $J = 8.1$ Hz, 2H, CH_2), 3.12 (t, $J = 8.1$ Hz, 2H, CH_2), 7.26 (dd, $J = 7.4, 7.4$ Hz, 1H, Ar-H), 7.42 (dd, $J = 7.9, 7.9$ Hz, 2H, Ar-H), 7.53 (d, $J = 8.8$ Hz, 2H, Ar-H), 7.61 (d, $J = 8.8$ Hz, 2H, Ar-H), 7.81–7.84 (m, 4H, Ar-H), 8.19 (d, $J = 9.2$ Hz, 2H, Ar-H), 10.45 (s, 1H, NH), 10.48 (s, 1H, NH). $^{13}\text{C-NMR}$ (125 MHz, $\text{DMSO-}d_6$): δ 22.17, 26.85, (119.98, $\text{CH} \times 2$), (119.25, $\text{CH} \times 2$), 124.49, (127.02, $\text{CH} \times 2$), 126.92, (128.10, $\text{CH} \times 2$), (128.21, $\text{CH} \times 2$), (128.48, $\text{CH} \times 2$), 131.25, 139.82, 141.98, 142.01, 148.60, 162.95, 178.98. EI-MS: (m/z, %): 445.18 (M^+ , 100), 446.19 ($\text{M}^+ + 1$, 27.81). Elemental analysis for $\text{C}_{23}\text{H}_{19}\text{N}_5\text{O}_3\text{S}$ (445.50), calcd.: C, 62.01; H, 4.30; N, 15.72. Found: C, 62.05; H, 4.34; N, 15.75.

1-(4-Nitrophenyl)-3-[4-(6-oxo-4,5-dihydropyridazin-3-yl)phenyl]urea (8e).

Yield (2.65 g, 75%); m.p. 294-296 °C; IR (KBr) cm^{-1} , 3364 (NH), 3164 (NH), 2970 (CH), 1655 (CO); $^1\text{H-NMR}$ (500 MHz, $\text{DMSO-}d_6$): δ 2.42 (t, $J = 8.2$ Hz, 2H, CH_2), 2.91 (t, $J = 8.2$ Hz, 2H, CH_2), 7.53 (d, $J = 8.7$ Hz, 2H, Ar-H), 7.68 (d, $J = 8.7$ Hz, 2H, Ar-H), 7.70 (d, $J = 8.9$ Hz, 2H, Ar-H), 8.19 (d, $J = 8.9$ Hz, 2H, Ar-H), 9.11 (s, 1H, NH), 9.48 (s, 1H, NH), 10.85 (s, 1H, NH). $^{13}\text{C-NMR}$ (125 MHz, $\text{DMSO-}d_6$): δ 21.52, 26.22, (117.22, CH \times 2), (118.02, CH \times 2), 125.99, (126.11, CH \times 2), (128.01, CH \times 2), 132.86, 140.88, 144.73, 145.81, 152.95, 165.92. EI-MS: (m/z, %): 353.18 (M^+ , 100), 354.16 (M^++1 , 19.83). Elemental analysis for $\text{C}_{17}\text{H}_{15}\text{N}_5\text{O}_4$ (353.34), calcd.: C, 57.79; H, 4.28; N, 19.82. Found: C, 57.75; H, 4.23; N, 19.85.

1-(4-Nitrophenyl)-3-[4-(6-oxo-1-phenyl-4,5-dihydropyridazin-3-yl)phenyl]urea (8f).

Yield (3.22 g, 75%); m.p. 296-298 °C; IR (KBr) cm^{-1} , 3353 (NH), 3158 (NH), 3102 (CH), 1648 (CO). $^1\text{H-NMR}$ (500 MHz, $\text{DMSO-}d_6$): δ 2.47 (t, $J = 8.1$ Hz, 2H, CH_2), 3.10 (t, $J = 8.1$ Hz, 2H, CH_2), 7.27 (dd, $J = 7.3, 7.3$ Hz, 1H, Ar-H), 7.41 (dd, $J = 8.1, 8.1$ Hz, 2H, Ar-H), 7.52–7.57 (m, 4H, Ar-H), 7.69 (d, $J = 8.1$ Hz, 2H, Ar-H), 7.80 (d, $J = 8.7$ Hz, 2H, Ar-H), 8.19 (d, $J = 8.7$ Hz, 2H, Ar-H), 9.18 (s, 1H), 9.48 (s, 1H, NH). $^{13}\text{C-NMR}$ (125 MHz, $\text{DMSO-}d_6$): δ 22.68, 27.38, (119.50, CH \times 2), (120.03, CH \times 2), 121.87, (122.02, CH \times 2), 125.97, (125.98, CH \times 2), (128.11, CH \times 2), (128.00, CH \times 2), 129.17, 139.30, 139.85, 140.13, 150.21, 152.09, 167.32. EI-MS: (m/z, %): 429.18 (M^+ , 100), 430.29 (M^++1 , 26.77). Elemental analysis for $\text{C}_{23}\text{H}_{19}\text{N}_5\text{O}_4$ (429.44), calcd.: C, 64.33; H, 4.46; N, 16.31. Found: C, 64.36; H, 4.50; N, 16.30.

1-(4-Chlorophenyl)-3-[4-(6-oxo-4,5-dihydropyridazin-3-yl)phenyl]urea (8g).

Yield (3.12 g, 72%); m.p. > 300 °C; IR (KBr) cm^{-1} , 3385 (NH), 3216 (NH), 3104 (NH), 2950 (CH), 1668 (CO). $^1\text{H-NMR}$ (500 MHz, $\text{DMSO-}d_6$): δ 2.41 (t, $J = 8.2$ Hz, 2H, CH_2), 2.90 (t, $J = 8.2$ Hz, 2H, CH_2), 7.31 (d, $J = 8.4$ Hz, 2H, Ar-H), 7.47 (d, $J = 8.4$ Hz, 2H, Ar-H), 7.49 (d, $J = 8.8$ Hz, 2H, Ar-H), 7.67 (d, $J = 8.8$ Hz, 2H, Ar-H), 8.87 (s, 1H, NH), 8.90 (s, 1H), 10.83 (s, 1H, NH). $^{13}\text{C-NMR}$ (125 MHz, $\text{DMSO-}d_6$): δ 21.70, 26.05, (117.77, CH \times 2), (119.81, CH \times 2), 125.49, (126.41, CH \times 2), (128.66, CH \times 2), 129.45, 138.57, 140.61, 142.09, 152.43, 166.98. EI-MS: (m/z, %): 342.23 (M^+ , 100), 344.21 (M^++2 , 33.78). Elemental analysis for $\text{C}_{17}\text{H}_{15}\text{ClN}_4\text{O}_2$ (342.78), calcd.: C, 59.57; H, 4.41; N, 16.35. Found: C, 59.62; H, 4.48; N, 16.31.

1-(4-Chlorophenyl)-3-[4-(6-oxo-1-phenyl-4,5-dihydropyridazin-3-yl)phenyl]urea (8h).

Yield (3.14 g, 75%); m.p. 273-275 °C; IR (KBr) cm^{-1} , 3357 (NH), 3297 (NH), 3130 (CH), 1651 (CO). $^1\text{H-NMR}$ (500 MHz, $\text{DMSO-}d_6$): δ 2.70 (t, $J = 8.1$ Hz, 2H, CH_2), 3.10 (t, $J = 8.1$ Hz, 2H, CH_2), 7.27

(dd, $J = 8.4, 8.4$ Hz, 1H, Ar-H), 7.42 (d, $J = 8.5$ Hz, 2H, Ar-H), 7.54-7.60 (m, 4H, Ar-H), 7.68 (d, $J = 8.5$ Hz, 2H, Ar-H), 7.79 (d, $J = 8.9$ Hz, 2H, Ar-H), 8.18 (d, $J = 8.9$ Hz, 2H, Ar-H), 9.18 (s, 1H, NH), 9.48 (s, 1H, NH). $^{13}\text{C-NMR}$ (100 MHz, DMSO- d_6): δ 22.49, 27.93, (118.24, CH \times 2), (120.32, CH \times 2), (125.34, CH \times 2), 126.01, 126.52, (127.44, CH \times 2), (128.76, CH \times 2), (129.14, CH \times 2), 129.22, 138.98, 141.64, 141.97, 152.18, 152.69, 165.80. EI-MS: (m/z, %): 418.23 (M^+ , 100), 420.91 ($\text{M}^+ + 2$, 33.38). Elemental analysis for $\text{C}_{23}\text{H}_{19}\text{ClN}_4\text{O}_2$ (418.88), calcd.: C, 65.95; H, 4.57; N, 13.38. Found: C, 65.90; H, 4.60; N, 13.41.

1-[4-(6-Oxo-4,5-dihydropyridazin-3-yl)phenyl]-3-(p-tolyl)urea (8i).

Yield (2.30 g, 71%); m.p. > 300 °C; IR (KBr) cm^{-1} , 3348 (NH), 3196 (NH), 3100 (NH), 2918 (CH), 1673 (CO). $^1\text{H-NMR}$ (500 MHz, DMSO- d_6): δ 2.23 (s, 3H, CH_3), 2.41 (t, $J = 8.2$ Hz, 2H, CH_2), 2.90 (t, $J = 8.2$ Hz, 2H, CH_2), 7.08 (d, $J = 8.3$ Hz, 2H, Ar-H), 7.32 (d, $J = 8.3$ Hz, 2H, Ar-H), 7.48 (d, $J = 8.70$ Hz, 2H, Ar-H), 7.67 (d, $J = 8.7$ Hz, 2H, Ar-H), 8.59 (s, 1H, NH), 8.80 (s, 1H, NH), 10.82 (s, 1H, NH). $^{13}\text{C-NMR}$ (125 MHz, DMSO- d_6): δ 20.36, 21.70, 26.07, (117.85, CH \times 2), (118.37, CH \times 2), (126.40, CH \times 2), (129.20, CH \times 2), 130.82, 136.93, 140.90, 142.09, 149.21, 152.37, 166.70. EI-MS: (m/z, %): 322.33 (M^+ , 100), 323.85 ($\text{M}^+ + 1$, 20.28). Elemental analysis for $\text{C}_{18}\text{H}_{18}\text{N}_4\text{O}_2$ (322.37), calcd.: C, 67.07; H, 5.63; N, 17.38. Found: C, 67.11; H, 5.68; N, 17.35.

5.2. Biological methodology

Five human tumor cell lines HCT-116, Hela, HEPG-2, MCF-7 and PC-3; were obtained from American Type Culture Collection (ATCC)⁵¹ via Holding company for biological products and vaccines (VACSERA), Cairo, Egypt. These cell lines were used to determine the inhibitory effects of compounds **4a–8i** on cell growth against the standard antitumor drug sorafenib.

5.2.1. MTT assay for cytotoxicity

MTT methodology⁵²⁻⁵⁵ is a colorimetric assay based on the conversion of the yellow tetrazolium bromide to a purple formazan⁵⁶ derivative by mitochondrial succinate dehydrogenase.⁵⁷ Cell lines were cultured in RPMI-1640 medium with 10% fetal bovine serum. 100 IU/mL Penicillin and 100 $\mu\text{g/mL}$ streptomycin were added at 37 °C in a 5% carbon dioxide incubator for 48 h. The cell lines were then seeded in a 96-well plate at a density of 10^4 cells/well. After incubation, the cells were treated with different concentrations of the designed compounds **4b–8i** and incubated for additional 24 h. Then, MTT (5 mg/mL, 20 μl) solution was added and incubated for another 4 h. Dimethyl sulfoxide (100 μl) was added into each well to dissolve the formed purple formazan. The colorimetric assay was

performed and results were measured and recorded at absorbance of 570 nm using a plate reader (EXL 800, USA). The relative cell viability was calculated as a percentage of (A₅₇₀ of treated samples/A₅₇₀ of untreated sample). The cytotoxic activity was expressed as IC₅₀ mean ± SEM compared with the growth of untreated cells.

5.2.2. *B-Raf inhibition assay*

The detecting reagent Kinase-Glo[®] MAX was used to measure B-Raf kinase activity. The B-Raf kinase assay kit was added to 96-well plates with purified recombinant B-Raf (V600E)^{44, 45} enzyme, B-Raf substrate, ATP and kinase assay buffer. After preparation of the positive control, test inhibitor and blank wells, diluted Raf (V600E) enzyme was added to both the positive control and test inhibitor with incubation for 45 minutes at 30 °C. Then, Kinase-Glo[®] MAX reagent was added to each well and incubated at room temperature for 15 minutes.⁵⁸ Measurement of the produced luminescence was performed *via* a micro-plate reader. All samples and controls were tested in duplicate.⁵⁹

5.2.3. *Cell cycle analysis*

The MCF-7 cell lines were treated with compound **8b** for 24 h. After that, the cells were suspended in 0.5 mL of phosphate buffer saline (PBS), collected by centrifugation, fixed with ice-cold ethanol (70% v/v), re-suspended with RNase (0.1 mg/mL), stained with propidium iodide (PI) (50 µg/mL) and incubated at 37 °C in a 5% carbon dioxide incubator for 55 min. The PI fluorescence intensity was measured by flow cytometry using FACS caliber (Becton Dickinson).^{60, 61}

5.2.4. *Detection of apoptosis*

The MCF-7 cell lines in complete growing medium were treated with compound **8b** and incubated for 24 h. Then, 1-5 X 10⁵ cells were harvested and suspended in 500 µL of 1X binding buffer after that, 5 µL of Annexin V-FITC and 5 µL of PI were added. The reaction media were then reincubated in dark for further 5 min. Analysis of Annexin-V-FITC binding was performed using FACS caliber flow cytometer.

5.3. *Molecular docking methodology*

Molecular docking was carried out using MOE software. The three-dimensional structures of the ligand compounds **4b-8i** were generated using Cambridge software program chem. office. The 3D crystal structure of the target protein 1UWJ was retrieved from the Protein Data Bank (PDB) at the

Research Collaboratory for Structural Bioinformatics (RCSB, <http://www.rcsb.org>) and was imported in the MOE program.

MOE program recognized the binding cavity of the pre-existed ligand sorafenib and all the tested ligands were docked in this cavity. The number of runs of ligands was set to 30 and the lowest energy aligned conformations were identified. In a similar way the poses of the tested ligands **4b-8i** were selected and compared.

5. 4. ADMET properties and Lipinski's rule of five

The physicochemical properties of compounds **6a**, **7g**, **8b** and sorafenib were calculated using MOE software by creating a new data base followed by importing the compounds in the form of mol2 files then, the selected descriptors were computed.

6. Acknowledgments

The authors gratefully acknowledge Mansoura University for the continues support as well as the Holding Company for Biological Products and Vaccines (VACSERA), Cairo, Egypt, for performing the biological screening.

7. References

1. Momenimovahed Z. and Salehiniya H., Epidemiological characteristics of and risk factors for breast cancer in the world, *Breast Canc. Targ. Ther.*, **2019**, 11 151–164.
2. Ghorab M., Alsaïd M., Soliman A. and Al-Mishari A., Benzo[g]quinazolin-based scaffold derivatives as dual EGFR/HER2 inhibitors, *J. Enz. Inhib. Med. Chem.*, **2018**, 33, 67–73.
3. Tao X., Duan Y., Chen L., Design, synthesis and biological evaluation of pyrazolyl-nitro imidazole derivatives as potential EGFR/HER-2 kinase inhibitors. *Bioorg. Med. Chem. Lett.*, **2016**, 26, 677–83.
4. Sooa R., Limb S., Syna N., Tenga R., Soong R., Mokd T. and Choe B., Immune checkpoint inhibitors in epidermal growth factor receptor mutant non-small cell lung cancer: Current controversies and future directions, *Lung Cancer*, **2018**, 115, 12–20.
5. Pessôa M., Alves S., Taranto A., Villar J., Blanco G. and Barbosa L., Selectivity analyses of γ -benzylidene digoxin derivatives to different Na, K-ATPase α isoforms: a molecular docking approach, *J. Enz. Inhib. Med. Chem.*, **2018**, 33, 85–97.
6. Aoki, Y. and Matsubara, Y., Ras/MAPK syndromes and childhood hemato-oncological diseases, *Int. J. Hematol.*, **2013**, 97, 30–36.

7. Dietrich J., Gokhale V., Wanga X., Hurley L. and Flynn G., Application of a novel [3+2] cycloaddition reaction to prepare substituted imidazoles and their use in the design of potent DFG-out allosteric B-Raf inhibitors, *Bioorg. Med. Chem.*, **2010**, 18, 292–304.
8. El-Gamal M. and Oh ch., Design and Synthesis of an Anticancer Diarylurea Derivative with Multiple-Kinase Inhibitory Effect, *Bull. Korean Chem. Soc.*, **2012**, 33, 1571–1576.
9. Hussain M., Baig M., Mahmoud H., Ulhag Z., Hoessli D., Khogeer Gh., Al-Sayed R. and Al-Aama J., BRAF gene: From human cancers to developmental syndromes, *Saudi J. Biolog. Sci.*, **2015**, 22, 359–373.
10. Ammar U., Abdel-Maksoud M. and Oh Ch., Recent advances of RAF (rapidly accelerated fibrosarcoma) inhibitors as anti-cancer agents, *Eur. J. Med. Chem.*, **2018**, 158, 144–166.
11. Wang Y., Nie H., Zhao X., Qin Y. and Gong X., Bicyclol induces cell cycle arrest and autophagy in HepG2 human hepatocellular carcinoma cells through the PI3K/AKT and Ras/Raf/MEK/ERK pathways, *BMC Cancer*, **2016**, 16, 742–757.
12. Köhler M., Ehrenfeld S., Halbach S., Lauinger M., Burk U., Reischmann N., Cheng Sh., Spohr C., Maria F., Köhler N., Ringwald K., Braun S., Peters C., Zeiser R., Reinheckel T. and Brummer T., B-Raf deficiency impairs tumor initiation and progression in a murine breast cancer model, *oncogen*, **2019**, 38, 1324–1339.
13. Abdel-Maksoud M., El-Gamal M., Gamal El-Din M. and Oh Ch., Design, synthesis, *in vitro* anticancer evaluation, kinase inhibitory effects, and pharmacokinetic profile of new 1,3,4-triarylpyrazole derivatives possessing terminal sulfonamide moiety, *J. Enz. Inhib. Med. Chem*, **2019**, 34, 97–109.
14. Kim J., Choi B., Im D., Jung H., Moon H., Aman W. and Hah J., Computer-aided design and synthesis of 3-carbonyl-5-phenyl-1H-pyrazole as highly selective and potent BRAF V600E and CRAF inhibitor, *J. Enz. Inhib. Med. Chem.*, **2019**, 34, 1314–1320.
15. Ravez S., Castillo-Aguilera O., Depreux P. and Goossens L., Quinazoline derivatives as anticancer drugs: a patent review (2011-2014), *Expert Opin. Ther. Pat.*, **2015**, 25, 789–804.
16. Paul W., Mathew G., Mark R., Sharlene L., Dan N., Valerie G., Michael J., Christopher M., Caroline S., David B. and Richard M., Mechanism of Activation of the RAF-ERK Signaling Pathway by Oncogenic Mutations of B-RAF, *Cell*, **2004**, 116, 855–867.
17. Liu, Y. and Gray, N., Rational design of inhibitors that bind to inactive kinase conformations, *Nat. Chem. Biol.*, **2006**, 2, 358–364.
18. Wenglow sky S., Moreno D., Laird E., Gloor S., Ren L., Risom T., Rudolph J., Sturgis H., Voegtli W., Pyrazolopyridine inhibitors of B-Raf V600E. Part 4: Rational design and kinase

- selectivity profile of cell potent type II inhibitors, *Bioorg. Med. Chem. Lett.*, **2012**, 22, 6237–6241.
19. Ghrab M., Alsaïd M., Soliman A. and Ragab F., VEGFR-2 inhibitors and apoptosis inducers: synthesis and molecular design of new benzo[g]quinazolin bearing benzenesulfonamide moiety, *J. Enz. Inhib. Med. Chem.*, **2017**, 32, 893–907.
 20. Martin M., Alam R., Betzi S., Ingles D., Zhu J. and Schönbrunn E., A Novel Approach to the Discovery of Small-Molecule Ligands of CDK2, *ChemBioChem*, **2012**, 13, 2128–2136.
 21. Ahmad T. and Eisen T., Kinase Inhibition with BAY 43–9006 in Renal Cell Carcinoma, *Clin. Canc. Res.*, **2004**, 10, 6388–6392.
 22. Dar A., Das T., Shokat K. and Cagan R., Chemical genetic discovery of targets and anti-targets for cancer polypharmacology, *Nature*, **2012**, 486, 80–84.
 23. Salem M., Guirguis D., El-Helw E., Ghareeb M. and Derbala H., Antioxidant Activity of Heterocyclic Compounds Derived from 4-(4-Acetamidophenyl)-4-oxo-but-2-enoic Acid, *Inter. J. Sci. Res.*, **2014**, 3, 274–282.
 24. Zhang Y., Sun F., Dan W. and Fang X., Friedel–Crafts Acylation Reactions of BN-Substituted Arenes, *J. Org. Chem.*, **2017**, 82, 12877–12887.
 25. Erum K., Daniel J., Sten O. and Douglas A., Friedel-Crafts Acylation with Amides, *J. Org. Chem.*, **2012**, 77, 5788–5793.
 26. Lee S., Kim J., Kweon D., Kang Y., Cho S., Kim S. and Yoon Y., Recent progress in pyridazin-3(2*H*)-ones chemistry, *Curr. Med. Chem.*, **2004**, 8, 1463–1480.
 27. Abouzid K., Hakeem M., Khalil O. and Maklad Y., Pyridazinone derivatives: design, synthesis, and *in vitro* vasorelaxant activity, *Bioorg. Med. Chem.*, **2008**, 382–389.
 28. Abou-Zeid K., Youssef K., Shaaban M., El-Telbany F. and Al-Zanfaly S., Synthesis of 6-(4-(substituted-amino)phenyl)-4,5-dihydropyridazin-3(2*H*)-ones as potential positive inotropic agents, *Eg. J. Pharm. Sci.*, **1998**, 38, 319–331.
 29. Curran C. and Ross A., 6-Phenyl-4,5-dihydro-3(2*H*)-pyridazinones: A series of hypotensive agents, *J. Med. Chem.*, **1974**, 17, 273–281.
 30. Pokhodylo N., Teslenko Y., Matychuk V. and Obushak M., Synthesis of 2,1-Benzisoxazoles by Nucleophilic Substitution of Hydrogen in Nitroarenes Activated by the Azole Ring, *Synthesis*, **2009**, 16, 2741–2748.
 31. Zeghada S., Bentabed-Ababsa Gh., Derdour A., Abdelmounim S., Domingo L., S'aez J., Roisnel Th., Nassare E. and Mongin F., combined experimental and theoretical study of the thermal cycloaddition of aryl azides with activated alkenes, *Org. Biomol. Chem.*, **2011**, 9, 4295–4305.

32. Gong H., Baathulaa K., Lv J., Cai G. and Zhou Ch., Synthesis and biological evaluation of Schiff base linked imidazolyl naphthalimides as novel potential anti-MRSA agents, *Med. Chem. Commun.*, **2016**, 10, 1038–1043.
33. Faidallah H., Rostom Sh. and Al-Saadi M., Synthesis and Biological Evaluation of Some New Substituted Fused Pyrazole Ring Systems as Possible Anticancer and Antimicrobial agents, *JKAU*, **2010**, 22, 177–191.
34. Davies H., Bignell G.R., Cox C., Stephens P., Edkins S., Clegg S., Teague J., Woffendin H., Garnett M.J., Bottomley W., Davis N., Dicks E., Ewing R., Floyd Y., Gray K., Hall S., Hawes R., Hughes J., *et al.*, Mutations of the BRAF gene in human cancer, *Nature*, **2002**, 417, 949–954.
35. Cantwell-Dorris E., O’Leary J. and Sheils O., BRAF^{V600E}: Implications for Carcinogenesis and Molecular Therapy, *Mol. Canc. Ther.*, **2011**, 10, 385–394.
36. Obaid N., Bedard K. and Huang W., Strategies for Overcoming Resistance in Tumours Harboring BRAF Mutations, *Int. J. Mol. Sci.*, **2017**, 18, 585–600.
37. Huang K., Chen Z., Liu Y., Li Z., Wei J., Wang M., Zhang G., and Liang H., Platinum(II) complexes with mono-aminophosphonate ester targeting group that induce apoptosis through G1 cell-cycle arrest: Synthesis, crystal structure and antitumour activity, *Eur. J Med. Chem.*, **2013**, 63, 76–84.
38. Bussiere, D., Xie, L., Srinivas, H., Shu, W., Burke, A., Be, C., Zhao, J., Godbole, A., King, D., Karki, R., Hornak, V., Xu, F., Cobb, J., Carte, N., Frank, A., Frommlet, A., Graff, P., Knapp, M., Fazal, A., Okram, B., Jiang, S., Michellys, P., Beckwith, R., Voshol, H., Wiesmann, C., Solomon, J. and Paulk, J., Structural basis of indisulam-mediated RBM39 recruitment to DCAF15 E3 ligase complex, *Nat. Chem. Biol.*, **2020**, 16, 15–23.
39. Kurniawati, S., Mertaniasih, N., Ato, M., Tamura, T., Soedarsono, S., Aulanni'am, A., Mori, S., Maeda, Y. and Mukai, T., Cloning and Protein Expression of eccB5 Gene in ESX-5 System from Mycobacterium tuberculosis, *BioRes. Op. acc.*, **2020**, 9, 86–93.
40. Tarver, T., Hill, J., Rahmat, L., Perl, A., Bahceci, E., Mori, K. and Smith, C., Gilteritinib is a clinically active FLT3 inhibitor with broad activity against FLT3 kinase domain mutations, *Blood Adv.*, **2020**, 4, 514–524.
41. Jabbarzadeh P., Ismail P. and Ling K., Molecular modeling, dynamics simulations and binding efficiency of berberine derivatives: A new group of RAF inhibitors for cancer treatment, *PLOS*, **2018**, 13, 1–19.

42. Sasikala P., Stela P. and Meena K., Molecular docking studies of B-RAF expression inhibitors identified from *Strychnos potatorum* (Thethankottai), *J. Comput. Meth. Mol. Des.*, **2015**, 5, 102–108.
43. Zhang W., Qiu, K., Yu F., Xie X., Zhang Sh., Chen Y. and Xie H., Virtual Screening of B-Raf Kinase Inhibitors: A Combination of Pharmacophore Modelling, Molecular Docking, 3D QSAR Model and Binding Free Energy Calculation Studies, *Comput. Biol. Chem.*, **2017**, 70, 186–190.
44. Ping Y., Jin Y., Du-shu H., Wei L., Na W., Shao-ping F., Qing-shan P., Ze-feng W., and Yong M., Docking Studies on a Series of Novel Potent BRAF Inhibitors", *Adv. Mat. Res.*, **2013**, 34, 930–933.
45. Irene C., Anke B., Steffen S., Heinz S., Gerd B., Otmar S., Pilar G., Andreas S., Norbert S., Christian H., Florian C., Sien M., Arno K., Norbert K., and Geunther A., A Novel RAF Kinase Inhibitor with DFG-Out Binding Mode: High Efficacy in BRAF-Mutant Tumor Xenograft Models in the Absence of Normal Tissue Hyperproliferation, *Mol. Cancer Ther.*, **2016**, 15, 354–356.
46. Maurizio P., Gabriella T, Chiara M., Michele M., Rosita L., Nadia A., Elena C., Nicoletta C., Luca C., Marina F., Fabio G., Wilma P., Alessandra S., Daniele D., Eduard F., Arturo G., Antonella I., Enrico P., and Marina C., Optimization of Diarylthiazole B-Raf Inhibitors: Identification of a Compound Endowed with High Oral Antitumor Activity, Mitigated hERG Inhibition, and Low Paradoxical Effect, *ChemMedChem*, **2015**, 10, 276–295.
47. Lipinski Ch., Lombardo F., Dominy B. and Feeney P, Experimental and computational approaches to estimate solubility and permeability in drug discovery and development settings, *Advan. Drug Deliv. Rev.*, **2001**, 46, 3–26.
48. Al-Salem H., Hegazy G., El-Taher K., El-Messery Sh., Al-Obaid A., El-Subbagh H., Synthesis, anticonvulsant activity and molecular modeling study of some new hydrazinecarbothioamide, benzenesulfonohydrazide, and phenacylaceto-hydrazide analogues of 4(3*H*)-quinazolinone, *Bioorg. Med. Chem. Lett.*, **2015**, 25, 1490–1499.
49. Molecular Operating Environment (MOE), 2013.08, Chemical Computing Group ULC, **2018**, 1010 Sherbooke St. West, Suite #910, Montreal, QC, Canada, H3A 2R7.
50. Thyges M., Lehmann H., Gries J., König H., Kretzschmar R., Kunze J., Lebkücher R. and Lenke D., 6-Aryl-4,5-dihydro-3(2*H*)-pyridazinones A New Class of Compounds with Platelet Aggregation Inhibiting and Hypotensive Activities, *J. Med. Chem.*, **1983**, 26, 800–807.
51. Clark W. and Geary D., The Story of the American Type Culture Collection – Its History and Development (1899-1973), *Appl. Microbio.*, **1974**, 17, 295–309.

52. Baker, M., Deceptive curcumin offers cautionary tale for chemists, *Nature*, **2017**, 541, 144–145.
53. Rekha, S. and Anila, E., In vitro cytotoxicity studies of surface modified CaS nanoparticles on L929 cell lines using MTT assay, *Materials lett.*, **2019**, 236, 637–639.
54. Chung D., Kim J.H., Kim J.K., Evaluation of MTT and Trypan Blue assays for radiation-induced cell viability test in HepG2 cells, *Int. J. Radiat. Res.*, **2015**, 13, 331–335.
55. Meerloo J., Kaspers G. and Cloos J., Cell sensitivity assays: The MTT assay, *Meth. mol. Biol.*, **2011**, 731, 237–245.
56. Altman F., Tetrazolium salts and formazans, *Prog. Histochem. Cytochem.*, **1976**, 9, 1–56.
57. Oyedotun K. and Lemire B., The quaternary structure of the *Saccharomyces cerevisiae* succinate dehydrogenase. Homology modeling, cofactor docking, and molecular dynamics simulation studies, *J. Biol. Chem.*, **2004**, 279, 9424–9431.
58. Ma H., Deacon S. and Horiuchi K., The challenge of selecting protein kinase assays for lead discovery optimization, *Expert Opin. Drug Discov.*, **2008**, 3, 607–621.
59. Bell R. and Storey K., Novel detection method for chemiluminescence derived from the Kinase-Glo luminescent kinase assay platform: Advantages over traditional microplate luminometers, *MethodsX*, **2014**, 1, 96–101.
60. Thornton T. and Rincon M., Non-classical P38 map kinase functions: Cell cycle checkpoints and survival, *Int. J. Biol. Sci.*, **2009**, 5, 44–52.
61. Nicoletti I., Migliorati G., Pagliacci M., Grignani F. and Riccardi C., A rapid and simple method for measuring thymocyte apoptosis by propidium iodide staining and flow cytometry, *J. Immunol. Methods*, **1991**, 139, 271–279.

Graphical Abstract**Design, Synthesis and Molecular Modeling of Phenyl Dihydropyridazinone Derivatives as B-Raf Inhibitors with Anticancer Activity**

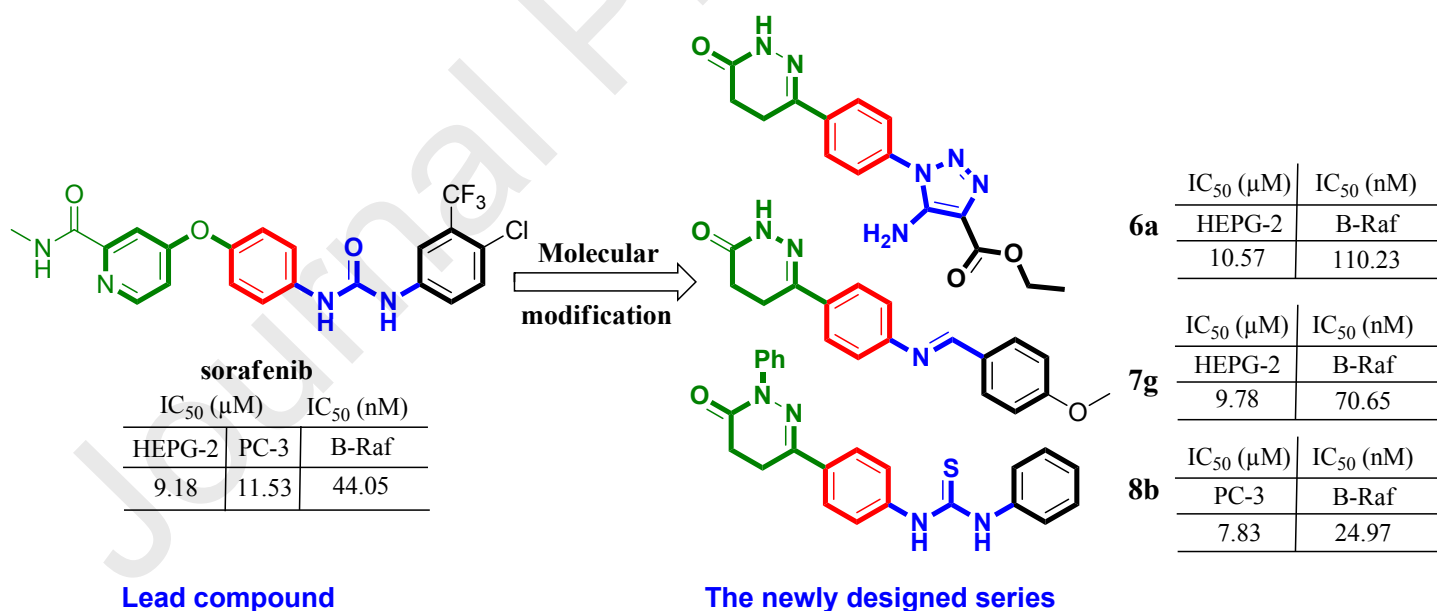
Mohamed G. Thabit,¹ Amany S. Mostafa,¹ Khalid B. Selim,^{1,*} Magda A. A. Elsayed^{1,2} and Magda N. A. Nasr¹

¹Department of Pharmaceutical Organic Chemistry, Faculty of Pharmacy, Mansoura University, Mansoura 35516, Egypt

²Department of Pharmaceutical Chemistry, Faculty of Pharmacy, Horus University, New Dammeitta, Egypt

*Corresponding author: K. B. Selim (e-mail: khbselim@mans.edu.eg)
tel: +2050-2247496 fax: +2050-2247496

Three series of pyridazinone derivatives were designed and synthesized as B-Raf kinase inhibitors. Nine compounds showed strong cytotoxic activity. Compounds **6a**, **7g** and **8b** showed potent inhibitory activity against B-Raf kinase. Further investigations were performed including molecular docking, cell cycle arrest and apoptosis.



Highlights

- New derivatives of hydropyridazinone were designed and synthesized as B-Raf kinase inhibitors.
- The synthesized compounds were evaluated for their antitumor activity against five selected cell lines.
- Compounds **6a**, **7g** and **8b** showed high inhibitory activity against B-Raf.
- Compound **8b** induced apoptosis and showed cell cycle arrest at G2/M phase.
- Molecular docking for the promising compounds was performed into B-Raf kinase binding site.